Studies on the Development of a Screening System for the Discovery of ALS Therapeutic Drugs and the Analysis of the Mechanism of Action of Acquired Compounds

January 2022

Yosuke KATO

Studies on the Development of a Screening System for the Discovery of ALS Therapeutic Drugs and the Analysis of the Mechanism of Action of Acquired Compounds

A Dissertation Submitted to

the Graduate School of Life and Environmental Sciences,

the University of Tsukuba

in Partial Fulfillment of the Requirements

for the Degree of Doctor of Philosophy in Science

(Doctoral Program in Biological Sciences)

Yosuke KATO

Table of Contents

Abbreviations

4-OHT	4-hydroxy tamoxifen
AAVS1	adeno-associated virus integration site 1
ALS	amyotrophic lateral sclerosis
BDNF	brain derived neurotrophic factor
ChAT	choline acetyltransferase
CNTF	ciliary neurotrophic factor
FGF	fibroblast growth factor
FTLD	frontotemporal lobar degeneration
GDNF	glial cell derived neurotrophic factor
hnRNP	heterogeneous nuclear ribonucleoprotein
iPS cell	induced pluripotent stem cell
MAP2	microtubule-associated protein 2
mTOR	mammalian target of rapamycin
NES	nuclear export signal
NLS	nuclear localization signal
PBS	phosphate buffered saline
PINK1	PTEN-induced putative kinase 1
ROS	reactive oxygen species
RRMs	RNA recognition motifs
STAT3	signal transducer and activator of transcription 3
TDP-43	TAR DNA-binding protein 43

1. Abstract

Amyotrophic lateral sclerosis (ALS) is characterized by progressive motor neuron loss in the brain and spinal cord; however, its etiology is unknown, and no curative treatment exists. TAR DNA-binding protein 43 (TDP-43), encoded by *TARDBP*, is a genetic mutation observed in 2-5% of familial ALS, and TDP-43 is known to be mislocalized in the cytoplasm. This study aimed to develop a screening system for compounds that inhibit the localization of TDP-43 from the nucleus to the cytoplasm using human induced pluripotent stem (iPS) cell-derived motor neurons with the aim of discovering therapeutic drugs for ALS. TDP-43 transgenic human iPS cells were constructed, differentiated into motor neurons, and then treated with MG-132 and sodium arsenite (stressors) to induce nuclear to cytoplasmic localization of TDP-43. STAT3 inhibitors, such as niclosamide, prevented TDP-43 mislocalization and degraded TDP-43 aggregates, and attenuated morphological changes under stress. Furthermore, niclosamide was found to inhibit ROS production and apoptosis, and to activate mitophagy via the PINK1-parkin-ubiquitin pathway. It was clarified that niclosamide exhibits a cytoprotective effect against stress by a combined action such as suppression of localization change of TDP-43 by inhibition of STAT3 and elimination mechanism of defective mitochondria by activation of mitophagy. The screening system based on TDP-43 localization change using human iPS cell-derived motor neurons are expected to pave the way for the development of ALS therapeutic drugs.

2. Introduction

Amyotrophic lateral sclerosis (ALS) is a neurodegenerative disease of unknown etiology that causes progressive respiratory muscle paralysis due to the degeneration of motor neurons that control muscles. Currently, there is no curative treatment for the disease (Hardiman et al. 2017; van Es et al. 2017). The progressive loss of motor neurons in the brain and spinal cord is a characteristic feature of ALS, which is also characterized by frontotemporal lobar degeneration (FTLD), a neurodegenerative pathological process. Interaction between various genetic and environmental factor have been implicated in the pathogenesis of the disease (Renton, Chio, and Traynor 2014). In 2006, TAR DNA-binding protein 43 (TDP-43) was reported as the major component protein in ubiquitin-positive inclusion bodies in patients with sporadic ALS (Arai et al. 2006; Neumann et al. 2006). TDP-43 positive inclusion bodies are also observed in FTLD-TDP (Geser et al. 2009). Mutations in TDP-43, encoded by the *TARDBP* gene, have been reported in ALS patients. Almost 90-95% ALS patients exhibit sporadic ALS (without a familial history). Among familial ALS patients, 2-5% exhibit mutations of the *TARDBP* gene and the remaining exhibit mutations in other genes, such as *SOD1*, *FUS,* and *C9ORF72* (Renton, Chio, and Traynor 2014). Neuronal inclusions in the brain and spinal cord of patients with ALS or FTLD-TDP contain phosphorylated and ubiquitinated TDP-43 protein (Prasad et al. 2019), suggesting that TDP-43 plays an important role in the pathogenesis of ALS.

TDP-43 is a 43 kDa protein consisting of 414 amino acids, expressed in organs throughout the body. As a heterogeneous nuclear ribonucleoprotein (hnRNP), TDP-43 is an RNA/DNA-binding protein that has two RNA recognition motifs (RRMs) and is involved in many processes of RNA metabolism such as transcription, translation, and splicing (Palomo et al. 2019; Prasad et al. 2019). About 30 types of missense mutations of TDP-43 are known (Lattante, Rouleau, and Kabashi 2013). TDP-43 is normally distributed in the nucleus; however, having a nuclear localization signal (NLS) and a nuclear export signal (NES), proteins can move between the cytoplasm and the nucleus. The proteins in ALS patients translocate from the nucleus to the cytoplasm and accumulate as abnormal insoluble aggregates in the cytoplasmic inclusion bodies (Lee, Lee, and Trojanowski 2011). In induced pluripotent stem (iPS) cell-derived motor neurons of ALS patients, the carboxyl-terminal fragment of TDP-43 is present in the cytoplasm, and is more aggregated than the full-length TDP-43, thus promoting TDP-43 aggregation and exhibiting cytotoxicity (Kitamura et al. 2016). The A90V mutation, involving the NLS region of TDP-43, has been reported to cause cytoplasmic mislocalization of TDP-43, decreasing protein solubility and forming insoluble aggregates, but pathological significance is unclear (Wobst et al. 2017). The M337V mutation also causes cytoplasmic mislocalization, which is enhanced by oxidative stress and is associated with apoptosis induction via caspase 3 activity (Mutihac et al. 2015). Insolubility of TDP-43 protein exerts inhibitory effects on the proteasome, thereby further stabilizing the protein and leading to

cytotoxicity (Watanabe, Kaneko, and Yamanaka 2013).

In ALS, the relation between TDP-43 regulated RNA metabolism and neurological disorders remains unclear. Neurodegeneration associated with TDP-43 is considered to result from the combined effects of protein toxicity and loss of normal TDP-43 functions (Lee, Lee, and Trojanowski 2011). Toxicity in neurons is induced by the accumulation of TDP-43 protein aggregates in the cytoplasm, and disruption of RNA metabolism occurs due to the loss of TDP-43 in the nucleus (Lee, Lee, and Trojanowski 2011). In its normal state, TDP-43 is expected to be degraded by the autophagy-ubiquitin-proteasome pathway (Prasad et al. 2019); however, the transfer of TDP-43 from the nucleus to the cytoplasm destabilizes the mRNA of the autophagic component, Atg7, leading to impairment of the autophagy process and promoting the accumulation of the ubiquitin-binding protein, p62, thereby contributing to the pathogenesis of the disease (Bose, Huang, and Shen 2011). In addition, stress granules formed by heat, oxidative stress, hypoxia, undernutrition, and viral infections are involved in the persistent accumulation of TDP-43 in the cytoplasm and are associated with the progression of neurodegenerative diseases such as ALS and FTLD (Fang et al. 2019). TDP-43 is therefore a promising target for the treatment of ALS; however, detailed elucidation of the molecular mechanism of TDP-43 is required.

Human iPS cells can produce large numbers of cells from patient tissues, and can be used to develop disease models that allow elucidation of the disease mechanism for drug

discovery/cell therapy. Human fibroblasts have been reprogrammed to generate iPS cells in patients with familial ALS, and a method for inducing differentiation of motor neurons has been established (Davis-Dusenbery et al. 2014; Sances et al. 2016). A model of ALS has been developed using iPS cell-derived motor neurons, and candidate compounds for the treatment of ALS are being screened. Digoxin-containing compounds are selected in drug screening by TDP-43 aggregates formation in motor neurons from ALS patients (Burkhardt et al. 2013). Anacardic acid, a histone acetyltransferase inhibitor, inhibits ALS motor neurons defects (Egawa et al. 2012). Veliparib, a PARP-1/2 inhibitor, reduces cytoplasmic TDP-43 aggregates formation (McGurk et al. 2018). Ropinirole, a dopamine D2 receptor agonist, is identified as a candidate compound based on phenotypic rescue screening used iPS cell-derived neurons of sporadic ALS patients (Fujimori et al. 2018).

This study aimed to develop a screening system for compounds that inhibit the localization of TDP-43 from the nucleus to the cytoplasm using human iPS cell-derived motor neurons discovering therapeutic drugs for ALS. TDP-43 transgenic human iPS cells were induced to differentiate into motor neurons. MG-132 (Klim et al. 2019; Watanabe, Kaneko, and Yamanaka 2013) and sodium arsenite (Egawa et al. 2012; Fang et al. 2019; McGurk et al. 2018), both of which have been reported to induce localization of TDP-43 from the nucleus to the cytoplasm, were used as stressors. Although neither stressor is endogenous, but the effects of MG-132 (proteasome inhibition) and sodium arsenite (oxidative stress induction) are assumed

to reproduce the cellular conditions in ALS pathology. Then, 946 selected compounds with known intracellular effects that inhibited the TDP-43 localization change were screened. An identified hit compounds were investigated to clarify the mechanism of TDP-43 mislocalization and attenuation of morphological changes under stress.

3. Materials and methods

3-1. Construction of TDP-43 transgenic human iPS cells and cell culture

Human iPS cells, strain A3 (F4V3-A3), were prepared using human dermal fibroblasts (Cell Applications, San Diego, CA, USA) (Yamashita et al. 2017). Human wild-type full-length *TDP-43* was introduced into the Cre-LoxP system and induced/expressed in human iPS cells. TDP-43 DNA fragment fused to *LoxP* and *mKate2* fluorescent gene and Cre-ERT2 DNA fragment were transduced into the adeno-associated virus integration site 1 (AAVS1) locus, the genomic safe harbor region, using genome editing technology. The cell line was then single-cloned. The iPS cells were cultured on collagen I-coated dish using Cellartis DEF-CS 500 Culture System (Takara Bio, Shiga, Japan). Cells were detouched by washing with D-phosphate buffered saline (PBS) (-/-), followed by treatment with TrypLE Select (Thermo Fisher Scientific, Waltham, MA, USA) and seeding into the dish.

3-2. Differentiation into motor neurons

Human iPS cells were differentiated into motor neurons in two steps, with slight modifications to previously reported methods (Klim et al. 2019). In step 1, iPS cells were differentiated into motor neuron progenitor cells, and in step 2, the progenitor cells were maturated into motor neurons.

The approach used in step 1 relies on neural induction through small molecule-mediated inhibition of SMAD signaling, accelerated iPS cells patterning through the activation of retinoic acid and Sonic Hedgehog signaling, and neural differentiation through inhibition of Notch and fibroblast growth factor (FGF) signaling (Klim et al. 2019). iPS cells were suspended in DEF-CS medium with 2.4 μM thiazovivin and 4.7 μg/mL fibronectin and were cultured on matrigel-coated dishes (day -1). The medium was replaced next day (day 0) with medium A (DMEM/F12 (Thermo Fisher Scientific), Neurobasal Plus (Thermo Fisher Scientific), penicillin-streptomycin (Sigma-Aldrich, Burlington, MA, USA), GlutaMax (Thermo Fisher Scientific), N-2 Supplement (Thermo Fisher Scientific), B-27 Plus Supplement (Thermo Fisher Scientific), 2 μM retinoic acid (Sigma-Aldrich), 1 μM SAG (Millipore, Burlington, MA, USA), 10 μM SB431542 (Sigma-Aldrich), and 1 μM dorsomorphin (Millipore)). Thereafter, the medium was replaced every other day (day 0-6). On day 6, the medium was replaced with medium B (DMEM/F12, Neurobasal Plus, penicillin-streptomycin, GlutaMax, N-2 Supplement, B-27 Plus Supplement, 2 μM retinoic acid, 1 μM SAG, 5 μM DAPT (Sigma-Aldrich), and 4 μM SU-5402 (BioVision, Zurich, Switzerland)). Thereafter, the medium was replaced every other day (day 6-10). Cells were harvested and cryopreserved on day 10 with DMEM/F12, Accutase (Thermo Fisher Scientific), 90 U/mL DNase I (Worthington, Lakewood, NJ, USA), and 9 U/mL papain (Worthington), and the cultures were passed through a 40 μm filter and centrifuged to collect the cells. The cells were suspended in Stem-Cellbanker

(Takara Bio) and stored at -150℃.

Step 2 was conducted as follows. Cryopreserved cells were thawed, suspended in maturation medium (Neurobasal Plus, Neuron Culture Medium (Fujifilm Wako, Osaka, Japan), N-2 Supplement, B-27 Plus Supplement, non-essential amino acids solution (Thermo Fisher Scientific), GlutaMax, penicillin-streptomycin, 10 ng/mL brain derived neurotrophic factor (BDNF) (Peprotech, Cranbury, NJ, USA), 10 ng/mL glial cell derived neurotrophic factor (GDNF) (R&D Systems, Minneapolis, MN, USA), 10 ng/mL ciliary neurotrophic factor (CNTF) (R&D Systems), and 6.2 μM L-ascorbic acid (Fujifilm Wako)), and cultured in poly-D-lysine and laminin-coated plates. Half of the medium was replaced twice a week.

3-3. Analysis of TDP-43 localization and neuronal morphology

The cells cryopreserved in step 1 were seeded in 96-well or 384-well plates and cultured in the maturation medium in step 2 (day 10). On day 13, half of the medium was changed and 100 nM 4-hydroxy tamoxifen (4-OHT) was added. Subsequently, on day 17, half the medium was changed, and a combination of a compound and a stressor (100 nM MG-132 (Fujifilm Wako) or 10 μM sodium arsenite (Santa Cruz Biotechnology, Dallas, TX, USA)) were added simultaneously. For screening, 946 compounds were obtained from Selleck, and stattic (Tocris Bioscience, Bristol, USA), niclosamide (Sigma-Aldrich), C188-9 (Merck, Darmstadt, Germany), S3I-201 (Seleck Chemicals, Huston, TX, USA), and nifuroxazide

(Sigma-Aldrich) were used for the confirmatory test. Cells were fixed with 4% paraformaldehyde for 20 min and rinsed three times with PBS. The cells were permeabilized with 0.1% Triton X-100 for 15 min and blocked with PBS containing 1% normal donkey serum, 1% bovine serum albumin (BSA), and 0.1% Triton X-100 for 1 hour. Anti-microtubule-associated protein 2 (MAP2) (ab32454, Abcam, Cambridge, UK) was incubated with PBS containing 1% normal donkey serum overnight at 4℃. The cells were rinsed with PBS, and anti IgG (H+L)-conjugated Alexa Fluor 488 (Thermo Fisher Scientific) and Hoechst 33342 (Dojindo, Kumamoto, Japan) were incubated with PBS containing 1% normal donkey serum for 1 hour. The fluorescence images were acquired using ArrayScan XTI (Thermo Fisher Scientific). The stained images by Hoechst 33342, anti-MAP2, and mKate2-TDP-43 were acquired in Blue (Ex 386/23 nm), Green (Ex 386/23 nm), and Red (Ex 560/25 nm) filters, respectively. TDP-43 localization was analyzed based on the colocalization measurement obtained in the HCS Studio Cellomics Scan (Thermo Fisher Scientific). The cytoplasmic region was stained by anti-MAP2 and the nuclear region was stained by Hoecht 33342, and TDP-43 expression either in the cytoplasm or in the nucleus enabled the analysis of cytoplasmic or nuclear localization. Neuronal profiling measurement in HCS Studio Cellomics Scan was used for neuronal morphology analysis. This method is based on the recognition of the neurite stained with anti-MAP2 and the calculation of the neurite length per neuron and the number of branch points per neuron.

3-4. Immunocytochemistry

Cells were fixed with 4% paraformaldehyde for 20 min and rinsed three times with PBS. The cells were permeabilized with 0.1% Triton X-100 for 15 min and blocked with PBS containing 1% normal donkey serum, 1% BSA, and 0.1% Triton X-100 for 1 hour. Primary antibodies were incubated with PBS containing 1% normal donkey serum overnight at 4℃. Primary antibodies used were as follows: anti-β-tubulin III (MAB1637, Millipore), anti-MAP2 (ab32454, Abcam), anti-choline acetyltransferase (ChAT) (ab181023, Abcam), anti-HB9 (sc-515769, Santa Cruz Biotechnology), anti-ISL1 (40.2 D6, DSHB, Iowa, IA, USA), and anti-BRN3A (AB5945, Millipore). The cells were rinsed with PBS, and incubated with secondary antibody in PBS containing 1% normal donkey serum for 1 hour. Secondary antibodies were as follows: anti-IgG (H+L) Conjugate Alexa Fluor 488 (Thermo Fisher Scientific). Nuclei were labeled with Hoechst 33342 and cells were rinsed with PBS. The fluorescence images were captured using fluorescence microscope, BZ-X810 (Keyence, Osaka, Japan).

3-5. Gene expression analysis

RNA was isolated using the RNeasy Plus Mini Kit (Qiagen, Venlo, Netherlands). The Luna Universal Probe One-Step RT-qPCR Kit (New England Biolabs, Ipswich, MA, USA) was used for quantitative PCR, and measurements were performed on the Step One Plus (Applied Biosystems). For the reaction, IDT Prime Time qPCR Probe was used (5‘dye: FAM, Quencher:

ZEN/IBFQ). Probes used were as follows: ChAT (Hs.PT.58.38606574), HB9 (Hs.PT.58.27510287), ISL1 (Hs.PT.58.2143768), BRN3A (Hs.PT.58.15720815), and GAPDH (Hs.PT.39a.22214836). Gene expression values were normalized using the GAPDH gene expression values.

3-6. Measurement of ATP, Caspase 3/7, ROS levels

Intracellular ATP levels were measured by CellTiter-Glo 2.0 Cell Viability Assay (Promega, Madison, WI, USA). Caspase 3/7 activities in the cells were measured by Caspase-Glo 3/7 assay (Promega). Reactive oxygen species (ROS) production in the cells was measured by the ROS-Glo H_2O_2 Assay (Promega). Luminescence quantification was performed with multi-plate reader, Envision 2103 (ParkinElmer, Waltham, MA, USA).

Fluorescence labeling of intracellular ROS was quantified by adding 5 μM CellROX Deep Red (Thermo Fisher Scientific) to the cells and incubating the cells at 37℃ for 30 min. The fluorescence images were captured by BZ-X810 (Keyence).

3-7. Western blot analysis

Cells were lysed in RIPA Buffer (Thermo Fisher Scientific) with Protease Phosphatase Inhibitor (Thermo Fisher Scientific) and treated with NuPAGE LDS Sample Buffer (Thermo Fisher Scientific) and NuPAGE Sample Reducing Agent (Thermo Fisher Scientific) at 95℃

for 5 min. Fractionation of insoluble and soluble TDP-43 was performed as follows. Cells were lysed in 1% sarkosyl, 10 mM Tris-HCl, 800 mM NaCl, and Protease Phosphatase Inhibitor. Cell lysates were ultrasonicated and ultracentrifuged at 100,000 x g for 30 min to separate into supernatant (a soluble fraction) and pellets (an insoluble fraction). The pellets were redissolved in RIPA buffer with the same volume with that of the corresponding supernatant. The protein concentration was determined by DC Protein AssayKit (Bio-Rad, Hercules, CA, USA) using BSA as a standard. SDS electrophoresis was performed using 4-20% TGX Gels (Bio-Rad) and the gels were blotted onto a PVDF membrane (Bio-Rad). The membrane was blocked with the PVDF Blocking Reagent (Toyobo, Osaka, Japan) and incubated with the following primary antibodies: anti-PTEN-induced putative kinase 1 (PINK1) (6946, Cell Signaling Technology, Danvers, MA, USA), anti-phospho-PINK1 (Ser228) (AF7081, Affinity Biosciences, Cincinnati, OH, USA), anti-parkin (4211, Cell Signaling Technology), anti-phospho-parkin (Ser65) (orb312554, Biorbyt, Cambridge, UK), anti-phospho-ubiquitin (Ser65) (62802, Cell Signaling Technology), anti-LC3 A/B (12741, Cell Signaling Technology), anti-SQSTM1/p62 (8025, Cell Signaling Technology), anti-signal transducer and activator of transcription 3 (STAT3) (4904, Cell Signaling Technology), anti-phospho-STAT3 (Tyr705) (9131, Cell Signaling Technology), anti-TDP-43 (ab190963, Abcam), and anti-GAPDH antibody (2118, Cell Signaling Technology). The membrane was then incubated with following peroxidase-conjugated secondary antibodies: anti-rabbit immunoglobulins/HRP (P0399, Dako, Santa

Clare, CA, USA) and anti-mouse immunoglobulins/HRP (P0447, Dako). And then, SuperSignal West Femto Maximum Sensitivity (Thermo Fisher Scientific) was added to detect luminescence using Amersham Imager 600 (GE Healthcare, Chicago, IL, USA).

4. Results

4-1. Differentiation of TDP-43 expressing human iPS cells into motor neurons

To screen for compounds that affect changes in the intracellular localization of TDP-43, the fluorescence-labeled *TDP-43* gene was transduced into iPS cells for simple and quantitative evaluation by fluorescence imaging. Human iPS cells, strain A3, to generate motor neurons. TDP-43 and Cre-ERT2 DNA fragments were transduced into the adeno-associated virus integration site 1 (AAVS1) locus, the safe harbor region of the genome, using genome editing technology. Addition of 4-hydroxy tamoxifen (4-OHT) to cells causes cleavage of *LoxP* by the Cre-LoxP system and induces expression of TDP-43 fused with mKate2 fluorescent protein by the CAG promoter (Fig. 1).

Differentiation from human iPS cells to motor neurons was performed separately in step 1 and step 2 (Fig. 2). In step 1, human iPS cels were differentiated into motor neuron progenitor cells, which were then differentiated for 10 days and cryopreserved. In step 2, the progenitor cells were cultured in the maturation medium to undergo maturation into motor neurons. The expression of marker genes specifically in motor neurons was confirmed by the presence of corresponding protein and mRNA. The expression of β-tubulin III and microtubule-associated protein 2 (MAP2), markers for mature neurons was confirmed by immunocytochemistry (Fig. 3). In addition, the expression of choline acetyltransferase (ChAT),

HB9, ISL1, and BRN3A, makers for motor neurons was confirmed by immunocytochemistry and gene expression analysis (Figs. 3 and 4). Based on this analysis, it was assumed that motor neuron maturation requires approximately 20 days of induction.

4-2. Establishment of screening system based on changes in the localization of TDP-43 and results of screening

Human iPS cell-derived motor neurons expressing TDP-43 were used to screen for compounds affecting localization changes of TDP-43. The cells cryopreserved in step 1 were seeded into 384-well plates to allow for the maturation of motor neurons in step 2. Induction of TDP-43 was initiated by addition of 100 nM 4-OHT on day 13, followed by the addition of 100 nM MG-132, a proteasome inhibitor (Klim et al. 2019; Watanabe, Kaneko, and Yamanaka 2013), on day 17. Cells were treated with MG-132 for 3 days. TDP-43 was expressed in the nucleus before MG-132 treatment, but overall expression decreased with MG-132 treatment and induced the expression spread to the cytoplasm (Fig. 5). Compounds affecting localization were screened by assessing TDP-43 expression levels in both cytoplasm and nucleus. Cell fixation was followed by cell staining and analyzed by fluorescence image analysis using Array scan XTI. Cytoplasm was stained with Alexa Fluor 488 labeled anti-MAP2 and nucleus was stained with Hoechst 33342. The percentage of differentiated cells obtained by this method, calculated as the ratio of the number of cells stained with anti-MAP2 to the total number of

cells stained with Hoechst 33342, was approximately 52% (data not shown). Expression of TDP-43 was divided into cytoplasmic and nuclear regions according to anti-MAP2 and Hoechst 33342 staining images (Fig. 6A). Total TDP-43 fluorescence area per cell was used for the cytoplasmic localization, and mean TDP-43 fluorescence intensity per cell was used for the nuclear localization. For the cytoplasmic localization, both total fluorescence area and mean fluorescence intensity showed similar results. Therefore, total fluorescence areas were used because it could obtain a less variable result. The change in the localization of TDP-43 in the presence or absence of stimulation was quantified, and both cytoplasmic and nuclear localization of TDP-43 were altered by MG-132 stimulation (Fig. 6B).

Since a screening system for compounds was established, the 946 selected compounds with known intracellular effects were evaluated. The cells were treated with 100 nM MG-132 and 5 μM compounds simultaneously, and cells were analyzed after 3 days. The inhibition was calculated from the changes compared with control (with MG-132) and blank (without MG-132). There were 7 compounds that showed activity for both cytoplasmic and nuclear localization changes, and IC50 was calculated for each activity (Table 1). The targets of hit compounds were signal transducer and activator of transcription 3 (STAT3) inhibitor (stattic), sodium channel inhibitor (digoxin, ouabain), and topoisomerase inhibitor (mitoxantrone, epirubicin, doxorubicin, daunorubicin). Among these compounds, I focused on STAT3 inhibition as a possible mechanism for drug discovery. Stattic and niclosamide are reported to

promote the differentiation of neuronal cells (Natarajan et al. 2014), but the effect of TDP-43 mislocalization is not clear. In this study, STAT3 inhibitors were investigated to clarify the mechanism of the TDP-43 mislocalization.

4-3. Niclosamide and stattic inhibit TDP-43 cytoplasmic and nuclear localization changes

Niclosamide, a STAT3 inhibitor, has been used clinically for more than 50 years as an anthelmintic (Ren et al. 2010). This study examined the effects of niclosamide and stattic on stress-induced localization changes of TDP-43 in human iPS cell-derived motor neurons. As stressors, 100 nM MG-132 or 10 μM sodium arsenite was used, both at concentrations sufficient to induce localization changes (Fig. 7).

Cells were treated with 100 nM MG-132 and the selected compounds simultaneously, and evaluated after 3 days. Niclosamide and stattic suppressed the expression of TDP-43 in the cytoplasm and prevented its disappearance from the nucleus (Figs. 8-11). The effect of sodium arsenite, which is known to induce oxidative stress, as a stressor (Egawa et al. 2012; Fang et al. 2019; McGurk et al. 2018) was then evaluated. Cells were treated with 10 μM sodium arsenite and the selected compounds simultaneously, and evaluated after 1 day. Niclosamide and stattic inhibited the changes in the cytoplasmic and nuclear localization of TDP-43, even in the case of sodium arsenite, indicating that the suppression of the TDP-43 localization

change was not specific to MG-132 (Figs. 12 and 13). Both compounds were seen to have a similar effect on localization changes of TDP-43, but stattic exhibited slight cytotoxicity based on observation of cell morphology (Fig. 11). Niclosamide was therefore selected to be used as a further validation compound. The effect of niclosamide on the mislocalization of TDP-43 was then investigated. Without MG-132, niclosamide had no significant effect on nuclear expression of TDP-43 (Figs. 14 and 15A). In addition, MG-132 was added prior to treatment with niclosamide. Cells were treated with MG-132 for 1 day and then added with MG-132 and niclosamide for 2 days, the inhibitory effect on mislocalization of TDP-43 was low. Niclosamide had a weak effect on localized changes that had already occurred, and it was assumed to act in the process of mislocalization (Fig. 15B).

Furthermore, TDP-43 expression was fractionated into soluble and insoluble fractions based on solubility in 1% sarkosyl. Stimulation with MG-132 increased insoluble TDP-43, and niclosamide strongly inhibited insoluble TDP-43 (Fig. 16). Niclosamide was shown to degrade MG-132 induced TDP-43 aggregates. Moreover, endogenous TDP-43 was expressed at much lower levels than overexpressed TDP-43, and MG-132 treatment did not insolubilize endogenous TDP-43 (Fig. 16). Therefore, the effect of endogenous TDP-43 expression on this study is expected to be minimal.

4-4. Niclosamide attenuates morphological changes under stress

Human iPS cell-derived motor neurons treated for 7 days induce cell damage more potently than treatment with 100 nM MG-132 for 3 days. The effect of niclosamide on cell damage was investigated by calculating the neurite length per neuron and the number of branch points per neuron based on anti-MAP2 staining images (Fig. 17).

Cells were treated with 100 nM MG-132 and niclosamide simultaneously, and evaluated after 3 days and 7 days. The number of neuronal cells were calculated from the number of nucleus co-stained with anti-MAP2. Treatment with MG-132 for 7 days caused a decrease in neuronal cells number compared to when cells were not treated with MG-132, showing that the damage to cells increased with MG-132 treatment time, and niclosamide slightly suppressed the decrease in the number of neuronal cells after 7 days of treatment (Fig. 18). As for TDP-43 localization changes, niclosamide suppressed the expression of TDP-43 in the cytoplasm and prevented its disappearance from the nucleus after 7 days of treatment as well as after 3 days of treatment (Fig. 18). Furthermore, by addition of niclosamide for 7 days, it was confirmed from stained with anti-MAP2 that the morphology (the neurite length and the number of branch points) of neurites was preserved by the treatment of MG-132 (Figs. 18 and 19). Niclosamide was thus found to be effective in alleviating morphological changes induced by MG-132.

4-5. Niclosamide decreases intracellular ATP and suppressed ROS production

The direct target molecule of niclosamide is unknown, but it inhibits JAK/STAT3, Wnt/β-catenin, and mammalian target of rapamycin (mTOR) signaling (Kadri, Lambourne, and Mehellou 2018). It also inhibits mitochondrial oxidative phosphorylation, leading to a reduction of intracellular ATP supply (Chen et al. 2018).

The mechanism of cell damage suppression by niclosamide under stress was elucidated by measuring intracellular ATP levels, caspase 3/7 activities, and reactive oxygen species (ROS) production in cells. Cells were treated with 100 nM MG-132 and niclosamide simultaneously, and evaluated after 3 days. Niclosamide suppressed intracellular ATP levels and caspase 3/7 activities (an indicator of apoptotic activities) in a dose-dependent manner (Fig. 20A). ROS production was assessed by measuring the production of H_2O_2 quantitatively using the ROS-Glo H_2O_2 assay. The production of H_2O_2 was decreased by the addition of niclosamide in a dose-dependent manner (Fig. 20A). However, since treatment with MG-132 for 3 days resulted in a slight increase in ROS production compared with control (with MG-132) and blank (without MG-132), the 7 days was also examined. After 7 days of treatment, ROS levels increased by MG-132 and were inhibited by niclosamide (Fig. 20B). Intracellular ROS was also evaluated by direct fluorescence detection using CellROX reagent. Cells were added with 100 nM MG-132 and niclosamide simultaneously, and evaluated after 1 day. A decrease in ROS

production was observed in the cells treated with niclosamide (Fig. 21). These results suggested that niclosamide minimizes the response to oxidative stress induced by MG-132 and suppresses ROS production.

4-6. Niclosamide activates PINK1-parkin-ubiquitin pathway to induce mitophagy and autophagy

The PTEN-induced putative kinase 1 (PINK1)-parkin pathway is known to eliminate mitochondria damaged induced by stress, and dysfunction of PINK1 and parkin has been reported as one of the causes of Parkinson's disease (Kazlauskaite and Muqit 2015). Niclosamide has been reported to activate the PINK1 pathway in Parkinson's disease cells model (Barini et al. 2018). The activation of the PINK1 pathway by niclosamide using human iPS cell-derived motor neurons was assessed.

Cells were treated with 100 nM 4-OHT to induce TDP-43 expression for 4 days, and then treated with 100 nM MG-132 and niclosamide simultaneously and evaluated after 3 days. Western blot analysis confirmed that niclosamide decreased the expression of STAT3 and phosphorylated STAT3 (Tyr705) in a dose-dependent manner and modulated STAT3 activity. STAT3 induces gene transcription, but the STAT3 gene itself is also a target, and positive feedback that directly binds to the recognition region of the STAT3 gene promoter and induces transcription has been reported (He et al. 2005). Therefore, along with the suppression of

phosphorylated STAT3 by niclosamide, STAT3 expression is also considered to be decreased (Fig. 22), and then the induction of mKate2-TDP-43 expression by 4-OHT was also demonstrated, and the overexpressed TDP-43 was also confirmed at the protein level (Fig. 22). Furthermore, niclosamide increased the expression of phosphorylated PINK1 (Ser228), phosphorylated parkin (Ser65), and phosphorylated ubiquitin (Ser65) (Fig. 23). In the PINK1-parkin-ubiquitin pathway, auto-phosphorylated PINK1 activates mitophagy by phosphorylating Ser65 of parkin and Ser65 of ubiquitin, which results in the degradation of damaged mitochondria (Kane et al. 2014; Koyano et al. 2014). It was suggested that niclosamide activates PINK1 and its downstream pathways, parkin and ubiquitin. In addition, niclosamide increased LC3 and decreased SQSTM1/p62, resulting in activation of autophagy (Fig. 23).

Next, in order to examine the relation between STAT3 activity and the PINK1-parkin-ubiquitin pathway, the localization changes of TDP-43 and the activation of PINK1 were examined using the following STAT3 inhibitors (stattic, C188-9, S3I-201, nifuroxazide) in addition to niclosamide. Cells were treated with 100 nM MG-132 and the STAT3 inhibitors simultaneously, and evaluated after 3 days. For changes in TDP-43 localization, all compounds suppressed TDP-43 expression in the cytoplasm. On the other hand, no effect was observed in TDP-43 expression in the nucleus other than niclosamide and stattic (Figs. 24 and 25). The nuclear TDP-43 expression is assumed to be retained due to factors other than STAT3 inhibition.

The western blot analysis showed that all compounds decreased the expression of phosphorylated STAT3 and were involved in the regulation of STAT3 (Fig. 26). Furthermore, only niclosamide increased the phosphorylation of ubiquitin, a mitophagy marker, and increased expression of LC3, an autophagy maker (Fig. 26). These results suggested that although STAT3 inhibition prevented mislocalization of TDP-43 in the cytoplasm, only niclosamide activated mitophagy and autophagy, suggesting an additional effect other than STAT3 inhibition.

5. Discussion

5-1. Development of a screening system based on mislocalization of TDP-43

In order to search for candidate compounds for ALS treatment, this study established the screening system based on changes of the localization of TDP-43 from the nucleus to the cytoplasm. Fluorescence-labeled TDP-43 was transduced into human iPS cells, and differentiated into motor neurons (Figs. 1-4). Proteasome inhibitor, MG-132, was added as a stressor to induce localization changes of TDP-43. In addition, analysis of the expression of TDP-43 by fractionation into soluble and insoluble fractions showed that MG-132 treatment decreased soluble TDP-43 and increased insoluble TDP-43 (Fig. 16), suggesting that overexpressed TDP-43 promoted stress-induced aggregates formation. This screening system enabled detection of TDP-43 localization changes for simple and quantitative evaluation by fluorescence imaging (Figs. 5 and 6). Furthermore, the use of human iPS cell-derived motor neurons may have provided an in vitro model that reproduces the intracellular signals and mechanisms affecting TDP-43 aggregation and degradation under conditions similar to those of human tissues. Therefore, the active compound obtained by this screening system is expected to have medicinal properties in humans.

5-2. Relationship between STAT3 inhibition and suppression of TDP-43 mislocalization

The 946 selected compounds with known intracellular effects that inhibited TDP-43 localization change were screened (Table 1). The hit compounds, niclosamide and stattic, prevented TDP-43 mislocalization, and niclosamide degraded TDP-43 aggregates (Figs. 9-13). In addition, niclosamide attenuated morphological changes under stress following treatment with MG-132 for 7 days (Figs. 17-19). Niclosamide and stattic are both STAT3 inhibitors, which control cell differentiation, survival, proliferation, and angiogenesis. Aberrantly activated STAT3 then induces tumor progression and is being investigated as a potential target for a variety of anti-cancer drugs (Beebe, Liu, and Zhang 2018). Niclosamide and stattic promote motor neurons differentiation in human neural stem cells (hNSCs) and inhibit the nuclear translocation of phosphorylated STAT3 (Natarajan et al. 2014). When STAT3 is transported into mitochondria, it suppresses the autophagy induced by oxidative stress, thereby inducing cell damage (You et al. 2015). In this study, C188-9, S3I-201, and nifuroxazide, which are STAT3 inhibitors like niclosamide and stattic, suppressed the localization of TDP-43 in the cytoplasm (Fig. 25). These results suggested that STAT3 inhibition is one of the effects affecting the mislocalization of TDP-43.

5-3. Relationship between the efficacy of niclosamide and cytoprotection against stress

Among the STAT3 inhibitors evaluated in this study, only niclosamide increased the expression levels of phosphorylated ubiquitin and LC3, suggesting the activation of mitophagy and autophagy (Figs. 23 and 26). Niclosamide has been used as an anthelmintic drug to treat tapeworm infection for more than 50 years and strongly inhibits the transcriptional activity of STAT3 and the proliferation of cancer cells in which STAT3 is constitutively activated (Ren et al. 2010). In addition to STAT3, niclosamide inhibits Wnt/β-catenin, mTOR, NF-kB, and Notch signaling, but the target molecule is unknown (Kadri, Lambourne, and Mehellou 2018; Li et al. 2014). In recent years, niclosamide is being investigated as a drug for the treatment of Parkinson's disease, type 2 diabetes, viral infection, microbial infection, neuropathic pain, rheumatoid arthritis, and systemic sclerosis besides as an anthelmintic (Chen et al. 2018; Kadri, Lambourne, and Mehellou 2018). However, while niclosamide is a safety drug with low systemic exposure, it has a poor pharmacokinetic profile, low aqueous solubility and a short half-life for oral administration, which may require improvement to expand the indication (Chen et al. 2018). The mechanism of action of niclosamide is reported to involve the inhibition of mitochondrial oxidative phosphorylation by uncoupling and the reduction of intracellular ATP supply (Chen et al. 2018), and niclosamide promotes lysosomal uptake and inhibits aggregates formation in neuroblastoma SH-SY5Y that expresses ubiquitin-fusion proteins

(Gies et al. 2010). In this study, niclosamide attenuated morphological changes under stress (Fig. 18), inhibited ROS production and apoptosis (Figs. 20 and 21), and activated mitophagy and autophagy (Fig. 23). Suppression of mislocalization of TDP-43 may have a cytoprotective effect against stress. However, in this study, STAT3 inhibitors suppressed mislocalization of TDP-43, but only niclosamide activated mitophagy and autophagy (Fig. 26). Therefore, although specific intracellular signals have not been identified, the cytoprotective effect against stress is likely due to a complex action other than STAT3 inhibition.

5-4. Mitophagy modulation as a potential therapeutic drug for ALS

Intracellular accumulation of abnormal protein aggregates is thought to be one of the causes of neurodegenerative diseases such as ALS, Parkinson's disease, Alzheimer's disease, and Huntington's disease (Renna et al. 2010). Increased clearance of proteins has been proposed as a therapeutic approach, and the autophagy-ubiquitin-proteasome pathway is the major degradation system for clearing unnecessary proteins (Jimenez-Sanchez et al. 2012). Upregulation of autophagy is expected to be a therapeutic strategy for neurodegenerative diseases (Renna et al. 2010). Furthermore, neurodegenerative diseases are characterized by loss of neuronal function and accumulation of toxic proteins that disturb cellular homeostasis. They induce mitochondrial dysfunction and are involved in the pathogenesis (Smith, Shaw, and De

Vos 2019).

Mitochondria are cell organelles essential for a variety of cellular processes, such as energy metabolism, calcium regulation, lipid biosynthesis, and apoptosis, therefore being indispensable to maintaining cellular homeostasis. Neurons are particularly energy dependent and are exposed to high levels of several ROS, thereby causing mitochondrial dysfunction to result in neuronal cell death emphasizing on the importance of multiple systems for mitochondrial quality control. Mitophagy is a selective form of autophagy in mitochondria, which degrades damaged mitochondria accurately (Pickles, Vigie, and Youle 2018; Youle and Narendra 2011) and its modulation may be a therapeutic approach for neurodegenerative diseases (Fivenson et al. 2017; Martinez-Vicente 2017; Rodolfo, Campello, and Cecconi 2018). *PINK1* and *parkin* have been identified as causative genes of an autosomal recessive form of familial early onset Parkinson's disease (Kazlauskaite and Muqit 2015). PINK1 and parkin modulate the removal of dysfunctional mitochondria through a mitophagy-mediated degradation pathway (Kazlauskaite and Muqit 2015; Yamano, Matsuda, and Tanaka 2016). PINK1 is a Ser/Thr kinase that accumulates on depolarized mitochondria, and parkin is an E3 ubiquitin ligase that catalyzes the transfer of ubiquitin to mitochondrial substrates. PINK1 acts upstream of parkin and is essential for the recruitment of parkin to activated and depolarized mitochondria. PINK1 auto-phosphorylates at Ser228 and Ser402 upon decrease in mitochondrial membrane potential, localizes parkin to mitochondria, phosphorylates and

activates Ser65 of parkin, and ubiquitinates damaged mitochondria (Okatsu et al. 2012). PINK1 also phosphorylates Ser65 of ubiquitin, which then activates parkin and activates E3 ubiquitin ligase (Kane et al. 2014). When both parkin and ubiquitin are phosphorylated in a PINK1-dependent manner, the activity of parkin is at the maximum, and the phosphorylated ubiquitin functions as an activator of parkin (Koyano et al. 2014; Matsuda 2016). The physiological relevance of phosphorylated ubiquitin is unknown; however, since ubiquitin phosphorylated at Ser65 is known to accumulate as intracellular granules in the mitochondria of the brain of elderly individuals, its application as a biomarker or therapeutic target is being investigated (Fiesel et al. 2015). The PINK1-parkin-ubiquitin pathway plays an important role in mitochondrial quality control, and the activation of mitophagy has been suggested to provide a neuroprotective effect (Lambourne and Mehellou 2018; Miller and Muqit 2019).

In this study, niclosamide reduced intracellular ATP production in mitochondria under stress, reduced oxidative stress response and apoptotic activity, and prevented cell damages (Figs. 20 and 21). Although attention should be paid to the possible cytotoxicity due to its effect on mitochondria. In addition, niclosamide increased phosphorylated PINK1, phosphorylated parkin, and phosphorylated ubiquitin (Fig. 23), indicating that activation of PINK1 leads to activation of downstream parkin and ubiquitin, and activation of mitophagy mediated by PINK1-parkin-ubiquitin pathway. The relationship between TDP-43/niclosamide and mitochondrial function has been reported as follows. TDP-43 induces cytoplasmic

accumulation of PINK1 by decreasing proteasome activity, resulting in impaired mitochondrial function (Sun et al. 2018). TDP-43 is normally partly present in mitochondria, where it controls appropriate levels of RNA intermediates, but TDP-43 with ALS mutation increases its abundance in mitochondria, and then overstabilizes RNA intermediates, inducing mitochondrial dysfunction and cell death (Izumikawa et al. 2017). Furthermore, niclosamide activates intracellular PINK1 and has shown potential as a candidate drug for Parkinson's disease (Barini et al. 2018). Considering the above, it is possible that niclosamide maintains mitochondrial function by suppressing the mislocalization of TDP-43 and regulates mitophagy by activating PINK1.

In summary, with the aim of discovering therapeutic drugs for ALS, a screening system for compounds that inhibit the localization of TDP-43 from the nucleus to the cytoplasm using human iPS cell-derived motor neurons were developed and compound screening was performed. The resulting STAT3 inhibitor, niclosamide, was analyzed and demonstrated for the first time that prevented TDP-43 mislocalization, degraded TDP-43 aggregates, activated mitophagy via the PINK1-parkin-ubiquitin pathway, and attenuated morphological changes under stress. It was clarified that niclosamide exhibits a cytoprotective effect against stress by a combined action such as suppression of localization change of TDP-43 by inhibition of STAT3 and elimination mechanism of defective mitochondria by activation of mitophagy. Although validation with niclosamide has not identified specific intracellular signals that

induce cytoprotective effects, it is important that this screening system enables us to obtain compounds that attenuate morphological changes under stress expected for discovering therapeutic drugs for ALS.

6. Acknowledgments

I would like to express my sincere appreciation to Associate Prof. Kazuichi Sakamoto for the generous guidance and support throughout this research.

I would also like to express my gratitude to all the members of the Sakamoto Laboratory at the University of Tsukuba for their advice and discussion at the progress report meeting.

Finally, I would like to express my sincere gratitude to all those who cooperated in carrying out this research.

7. References

Arai, T., M. Hasegawa, H. Akiyama, K. Ikeda, T. Nonaka, H. Mori, D. Mann, K. Tsuchiya, M. Yoshida, Y. Hashizume, and T. Oda. 2006. 'TDP-43 is a component of ubiquitin-positive tau-negative inclusions in frontotemporal lobar degeneration and amyotrophic lateral sclerosis', *Biochem Biophys Res Commun*, 351: 602-11.

Barini, E., A. Miccoli, F. Tinarelli, K. Mulholland, H. Kadri, F. Khanim, L. Stojanovski, K. D. Read, K. Burness, J. J. Blow, Y. Mehellou, and M. M. K. Muqit. 2018. 'The Anthelmintic Drug Niclosamide and Its Analogues Activate the Parkinson's Disease Associated Protein Kinase PINK1', *Chembiochem*, 19: 425-29.

Beebe, J. D., J. Y. Liu, and J. T. Zhang. 2018. 'Two decades of research in discovery of anticancer drugs targeting STAT3, how close are we?', *Pharmacol Ther*, 191: 74-91.

Bose, J. K., C. C. Huang, and C. K. Shen. 2011. 'Regulation of autophagy by neuropathological protein TDP-43', *J Biol Chem*, 286: 44441-8.

Burkhardt, M. F., F. J. Martinez, S. Wright, C. Ramos, D. Volfson, M. Mason, J. Garnes, V. Dang, J. Lievers, U. Shoukat-Mumtaz, R. Martinez, H. Gai, R. Blake, E. Vaisberg, M. Grskovic, C. Johnson, S. Irion, J. Bright, B. Cooper, L. Nguyen, I. Griswold-Prenner, and A. Javaherian. 2013. 'A cellular model for sporadic ALS using patient-derived induced pluripotent stem cells', *Mol Cell Neurosci*, 56: 355-64.

Chen, W., R. A. Mook, Jr., R. T. Premont, and J. Wang. 2018. 'Niclosamide: Beyond an

antihelminthic drug', *Cell Signal*, 41: 89-96.

Davis-Dusenbery, B. N., L. A. Williams, J. R. Klim, and K. Eggan. 2014. 'How to make spinal motor neurons', *Development*, 141: 491-501.

Egawa, N., S. Kitaoka, K. Tsukita, M. Naitoh, K. Takahashi, T. Yamamoto, F. Adachi, T. Kondo, K. Okita, I. Asaka, T. Aoi, A. Watanabe, Y. Yamada, A. Morizane, J. Takahashi, T. Ayaki, H. Ito, K. Yoshikawa, S. Yamawaki, S. Suzuki, D. Watanabe, H. Hioki, T. Kaneko, K. Makioka, K. Okamoto, H. Takuma, A. Tamaoka, K. Hasegawa, T. Nonaka, M. Hasegawa, A. Kawata, M. Yoshida, T. Nakahata, R. Takahashi, M. C. Marchetto, F. H. Gage, S. Yamanaka, and H. Inoue. 2012. 'Drug screening for ALS using patient-specific induced pluripotent stem cells', *Sci Transl Med*, 4: 145ra04.

Fang, M. Y., S. Markmiller, A. Q. Vu, A. Javaherian, W. E. Dowdle, P. Jolivet, P. J. Bushway, N. A. Castello, A. Baral, M. Y. Chan, J. W. Linsley, D. Linsley, M. Mercola, S. Finkbeiner, E. Lecuyer, J. W. Lewcock, and G. W. Yeo. 2019. 'Small-Molecule Modulation of TDP-43 Recruitment to Stress Granules Prevents Persistent TDP-43 Accumulation in ALS/FTD', *Neuron*, 103: 802-19 e11.

Fiesel, F. C., M. Ando, R. Hudec, A. R. Hill, M. Castanedes-Casey, T. R. Caulfield, E. L. Moussaud-Lamodiere, J. N. Stankowski, P. O. Bauer, O. Lorenzo-Betancor, I. Ferrer, J. M. Arbelo, J. Siuda, L. Chen, V. L. Dawson, T. M. Dawson, Z. K. Wszolek, O. A. Ross, D. W. Dickson, and W. Springer. 2015. '(Patho-)physiological relevance of

PINK1-dependent ubiquitin phosphorylation', *EMBO Rep*, 16: 1114-30.

Fivenson, E. M., S. Lautrup, N. Sun, M. Scheibye-Knudsen, T. Stevnsner, H. Nilsen, V. A. Bohr, and E. F. Fang. 2017. 'Mitophagy in neurodegeneration and aging', *Neurochem Int*, 109: 202-09.

Fujimori, K., M. Ishikawa, A. Otomo, N. Atsuta, R. Nakamura, T. Akiyama, S. Hadano, M. Aoki, H. Saya, G. Sobue, and H. Okano. 2018. 'Modeling sporadic ALS in iPSC-derived motor neurons identifies a potential therapeutic agent', *Nat Med*, 24: 1579-89.

Geser, F., M. Martinez-Lage, L. K. Kwong, V. M. Lee, and J. Q. Trojanowski. 2009. 'Amyotrophic lateral sclerosis, frontotemporal dementia and beyond: the TDP-43 diseases', *J Neurol*, 256: 1205-14.

Gies, E., I. Wilde, J. M. Winget, M. Brack, B. Rotblat, C. A. Novoa, A. D. Balgi, P. H. Sorensen, M. Roberge, and T. Mayor. 2010. 'Niclosamide prevents the formation of large ubiquitin-containing aggregates caused by proteasome inhibition', *PLoS One*, 5: e14410.

Hardiman, O., A. Al-Chalabi, A. Chio, E. M. Corr, G. Logroscino, W. Robberecht, P. J. Shaw, Z. Simmons, and L. H. van den Berg. 2017. 'Amyotrophic lateral sclerosis', *Nat Rev Dis Primers*, 3: 17071.

He, F., W. Ge, K. Martinowich, S. Becker-Catania, V. Coskun, W. Zhu, H. Wu, D. Castro, F. Guillemot, G. Fan, J. de Vellis, and Y. E. Sun. 2005. 'A positive autoregulatory loop of

Jak-STAT signaling controls the onset of astrogliogenesis', *Nat Neurosci*, 8: 616-25.

Izumikawa, K., Y. Nobe, H. Yoshikawa, H. Ishikawa, Y. Miura, H. Nakayama, T. Nonaka, M. Hasegawa, N. Egawa, H. Inoue, K. Nishikawa, K. Yamano, R. J. Simpson, M. Taoka, Y. Yamauchi, T. Isobe, and N. Takahashi. 2017. 'TDP-43 stabilises the processing intermediates of mitochondrial transcripts', *Sci Rep*, 7: 7709.

Jimenez-Sanchez, M., F. Thomson, E. Zavodszky, and D. C. Rubinsztein. 2012. 'Autophagy and polyglutamine diseases', *Prog Neurobiol*, 97: 67-82.

Kadri, H., O. A. Lambourne, and Y. Mehellou. 2018. 'Niclosamide, a Drug with Many (Re)purposes', *ChemMedChem*, 13: 1088-91.

Kane, L. A., M. Lazarou, A. I. Fogel, Y. Li, K. Yamano, S. A. Sarraf, S. Banerjee, and R. J. Youle. 2014. 'PINK1 phosphorylates ubiquitin to activate Parkin E3 ubiquitin ligase activity', *J Cell Biol*, 205: 143-53.

Kazlauskaite, A., and M. M. Muqit. 2015. 'PINK1 and Parkin - mitochondrial interplay between phosphorylation and ubiquitylation in Parkinson's disease', *FEBS J*, 282: 215-23.

Kitamura, A., Y. Nakayama, A. Shibasaki, A. Taki, S. Yuno, K. Takeda, M. Yahara, N. Tanabe, and M. Kinjo. 2016. 'Interaction of RNA with a C-terminal fragment of the amyotrophic lateral sclerosis-associated TDP43 reduces cytotoxicity', *Sci Rep*, 6: 19230.

Klim, J. R., L. A. Williams, F. Limone, I. Guerra San Juan, B. N. Davis-Dusenbery, D. A. Mordes, A. Burberry, M. J. Steinbaugh, K. K. Gamage, R. Kirchner, R. Moccia, S. H. Cassel, K. Chen, B. J. Wainger, C. J. Woolf, and K. Eggan. 2019. 'ALS-implicated protein TDP-43 sustains levels of STMN2, a mediator of motor neuron growth and repair', *Nat Neurosci*, 22: 167-79.

Koyano, F., K. Okatsu, H. Kosako, Y. Tamura, E. Go, M. Kimura, Y. Kimura, H. Tsuchiya, H. Yoshihara, T. Hirokawa, T. Endo, E. A. Fon, J. F. Trempe, Y. Saeki, K. Tanaka, and N. Matsuda. 2014. 'Ubiquitin is phosphorylated by PINK1 to activate parkin', *Nature*, 510: 162-6.

Lambourne, O. A., and Y. Mehellou. 2018. 'Chemical Strategies for Activating PINK1, a Protein Kinase Mutated in Parkinson's Disease', *Chembiochem*, 19: 2433-37.

Lattante, S., G. A. Rouleau, and E. Kabashi. 2013. 'TARDBP and FUS mutations associated with amyotrophic lateral sclerosis: summary and update', *Hum Mutat*, 34: 812-26.

Lee, E. B., V. M. Lee, and J. Q. Trojanowski. 2011. 'Gains or losses: molecular mechanisms of TDP43-mediated neurodegeneration', *Nat Rev Neurosci*, 13: 38-50.

Li, Y., P. K. Li, M. J. Roberts, R. C. Arend, R. S. Samant, and D. J. Buchsbaum. 2014. 'Multi-targeted therapy of cancer by niclosamide: A new application for an old drug', *Cancer Lett*, 349: 8-14.

Martinez-Vicente, M. 2017. 'Neuronal Mitophagy in Neurodegenerative Diseases', *Front Mol*

Neurosci, 10: 64.

Matsuda, N. 2016. 'Phospho-ubiquitin: upending the PINK-Parkin-ubiquitin cascade', *J Biochem*, 159: 379-85.

McGurk, L., J. Mojsilovic-Petrovic, V. M. Van Deerlin, J. Shorter, R. G. Kalb, V. M. Lee, J. Q. Trojanowski, E. B. Lee, and N. M. Bonini. 2018. 'Nuclear poly(ADP-ribose) activity is a therapeutic target in amyotrophic lateral sclerosis', *Acta Neuropathol Commun*, 6: 84.

Miller, S., and M. M. K. Muqit. 2019. 'Therapeutic approaches to enhance PINK1/Parkin mediated mitophagy for the treatment of Parkinson's disease', *Neurosci Lett*, 705: 7-13.

Mutihac, R., J. Alegre-Abarrategui, D. Gordon, L. Farrimond, M. Yamasaki-Mann, K. Talbot, and R. Wade-Martins. 2015. 'TARDBP pathogenic mutations increase cytoplasmic translocation of TDP-43 and cause reduction of endoplasmic reticulum Ca(2)(+) signaling in motor neurons', *Neurobiol Dis*, 75: 64-77.

Natarajan, R., V. Singal, R. Benes, J. Gao, H. Chan, H. Chen, Y. Yu, J. Zhou, and P. Wu. 2014. 'STAT3 modulation to enhance motor neuron differentiation in human neural stem cells', *PLoS One*, 9: e100405.

Neumann, M., D. M. Sampathu, L. K. Kwong, A. C. Truax, M. C. Micsenyi, T. T. Chou, J. Bruce, T. Schuck, M. Grossman, C. M. Clark, L. F. McCluskey, B. L. Miller, E.

Masliah, I. R. Mackenzie, H. Feldman, W. Feiden, H. A. Kretzschmar, J. Q. Trojanowski, and V. M. Lee. 2006. 'Ubiquitinated TDP-43 in frontotemporal lobar degeneration and amyotrophic lateral sclerosis', *Science*, 314: 130-3.

Okatsu, K., T. Oka, M. Iguchi, K. Imamura, H. Kosako, N. Tani, M. Kimura, E. Go, F. Koyano, M. Funayama, K. Shiba-Fukushima, S. Sato, H. Shimizu, Y. Fukunaga, H. Taniguchi, M. Komatsu, N. Hattori, K. Mihara, K. Tanaka, and N. Matsuda. 2012. 'PINK1 autophosphorylation upon membrane potential dissipation is essential for Parkin recruitment to damaged mitochondria', *Nat Commun*, 3: 1016.

Palomo, V., C. Tosat-Bitrian, V. Nozal, S. Nagaraj, A. Martin-Requero, and A. Martinez. 2019. 'TDP-43: A Key Therapeutic Target beyond Amyotrophic Lateral Sclerosis', *ACS Chem Neurosci*, 10: 1183-96.

Pickles, S., P. Vigie, and R. J. Youle. 2018. 'Mitophagy and Quality Control Mechanisms in Mitochondrial Maintenance', *Curr Biol*, 28: R170-R85.

Prasad, A., V. Bharathi, V. Sivalingam, A. Girdhar, and B. K. Patel. 2019. 'Molecular Mechanisms of TDP-43 Misfolding and Pathology in Amyotrophic Lateral Sclerosis', *Front Mol Neurosci*, 12: 25.

Ren, X., L. Duan, Q. He, Z. Zhang, Y. Zhou, D. Wu, J. Pan, D. Pei, and K. Ding. 2010. 'Identification of Niclosamide as a New Small-Molecule Inhibitor of the STAT3 Signaling Pathway', *ACS Med Chem Lett*, 1: 454-9.

Renna, M., M. Jimenez-Sanchez, S. Sarkar, and D. C. Rubinsztein. 2010. 'Chemical inducers of autophagy that enhance the clearance of mutant proteins in neurodegenerative diseases', *J Biol Chem*, 285: 11061-7.

Renton, A. E., A. Chio, and B. J. Traynor. 2014. 'State of play in amyotrophic lateral sclerosis genetics', *Nat Neurosci*, 17: 17-23.

Rodolfo, C., S. Campello, and F. Cecconi. 2018. 'Mitophagy in neurodegenerative diseases', *Neurochem Int*, 117: 156-66.

Sances, S., L. I. Bruijn, S. Chandran, K. Eggan, R. Ho, J. R. Klim, M. R. Livesey, E. Lowry, J. D. Macklis, D. Rushton, C. Sadegh, D. Sareen, H. Wichterle, S. C. Zhang, and C. N. Svendsen. 2016. 'Modeling ALS with motor neurons derived from human induced pluripotent stem cells', *Nat Neurosci*, 19: 542-53.

Smith, E. F., P. J. Shaw, and K. J. De Vos. 2019. 'The role of mitochondria in amyotrophic lateral sclerosis', *Neurosci Lett*, 710: 132933.

Sun, X., Y. Duan, C. Qin, J. C. Li, G. Duan, X. Deng, J. Ni, X. Cao, K. Xiang, K. Tian, C. H. Chen, A. Li, and Y. Fang. 2018. 'Distinct multilevel misregulations of Parkin and PINK1 revealed in cell and animal models of TDP-43 proteinopathy', *Cell Death Dis*, 9: 953.

van Es, M. A., O. Hardiman, A. Chio, A. Al-Chalabi, R. J. Pasterkamp, J. H. Veldink, and L. H. van den Berg. 2017. 'Amyotrophic lateral sclerosis', *Lancet*, 390: 2084-98.

Watanabe, S., K. Kaneko, and K. Yamanaka. 2013. 'Accelerated disease onset with stabilized familial amyotrophic lateral sclerosis (ALS)-linked mutant TDP-43 proteins', *J Biol Chem*, 288: 3641-54.

Wobst, H. J., S. S. Wesolowski, J. Chadchankar, L. Delsing, S. Jacobsen, J. Mukherjee, T. Z. Deeb, J. Dunlop, N. J. Brandon, and S. J. Moss. 2017. 'Cytoplasmic Relocalization of TAR DNA-Binding Protein 43 Is Not Sufficient to Reproduce Cellular Pathologies Associated with ALS In vitro', *Front Mol Neurosci*, 10: 46.

Yamano, Koji, Noriyuki Matsuda, and Keiji Tanaka. 2016. 'The ubiquitin signal and autophagy: an orchestrated dance leading to mitochondrial degradation', *EMBO reports*, 17: 300-16.

Yamashita, T., Y. Miyamoto, Y. Bando, T. Ono, S. Kobayashi, A. Doi, T. Araki, Y. Kato, T. Shirakawa, Y. Suzuki, J. Yamauchi, S. Yoshida, and N. Sato. 2017. 'Differentiation of oligodendrocyte progenitor cells from dissociated monolayer and feeder-free cultured pluripotent stem cells', *PLoS One*, 12: e0171947.

You, L., Z. Wang, H. Li, J. Shou, Z. Jing, J. Xie, X. Sui, H. Pan, and W. Han. 2015. 'The role of STAT3 in autophagy', *Autophagy*, 11: 729-39.

Youle, R. J., and D. P. Narendra. 2011. 'Mechanisms of mitophagy', *Nat Rev Mol Cell Biol*, 12: 9-14.

Table

Table 1. Inhibitory activities (IC50) of the compounds with regard to TDP-43 localization change and target classification for 7 hit compounds.

Compound	Target	IC50 (mM)	
		Cytoplasmic localization change	Nuclear localization change
Digoxin	Sodium channel inhibitor	0.021	0.20
Ouabain	Sodium channel inhibitor	0.028	0.13
Mitoxantrone	Topoisomerase inhibitor	0.31	0.88
Epirubicin	Topoisomerase inhibitor	0.47	2.97
Doxorubicin	Topoisomerase inhibitor	0.54	0.64
Stattic	STAT3 inhibitor	1.27	2.38
Daunorubicin	Topoisomerase inhibitor	1.92	0.57

Figures

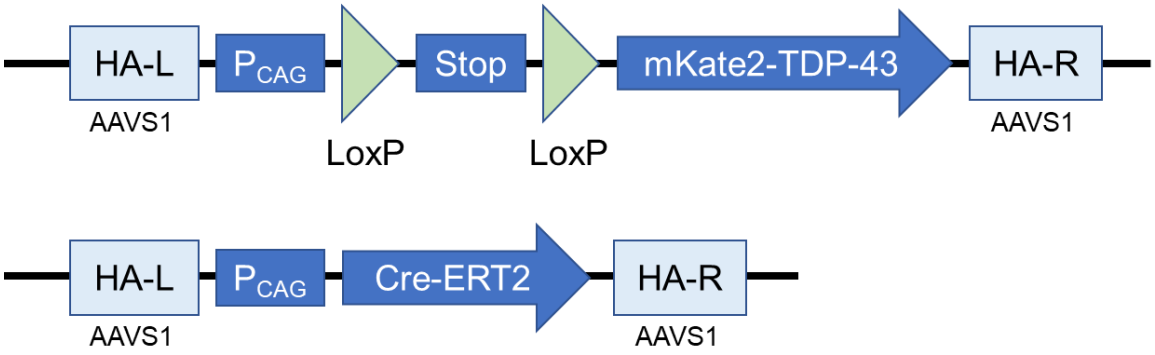

Figure 1. TDP-43 gene expression construct at the AAVS1 locus in the Cre-LoxP system of human iPS cells.

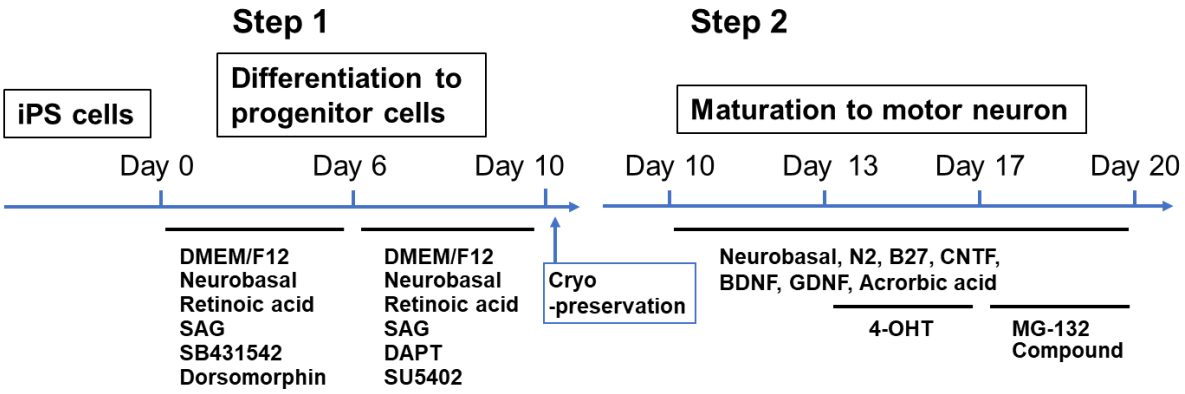

Figure 2. Protocol for human iPS cells differentiation into motor neurons.

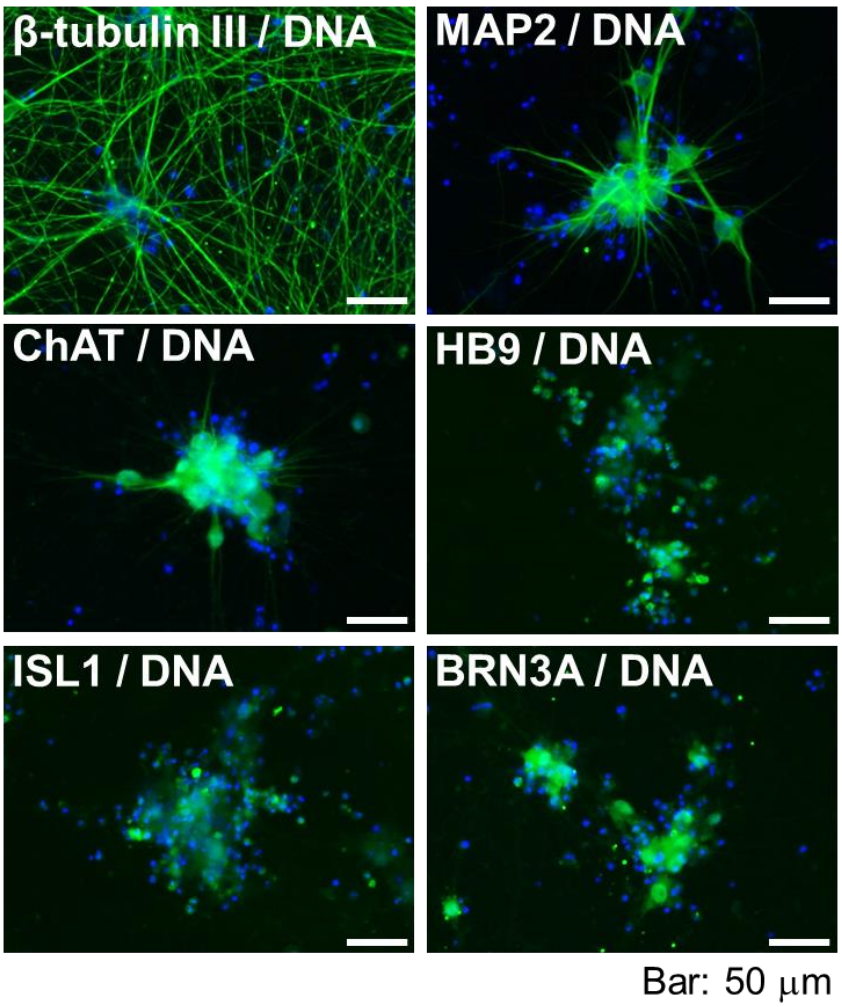

Figure 3. Immunocytochemical analysis at 50 days after motor neuron induction followed by cell fixation and staining.

Anti-β-tubulin III and anti-MAP2 were used as marker proteins for mature neurons. Anti-ChAT, anti-HB9, anti-ISL1, and anti-BRN3A were used as marker proteins for motor neurons. Scale bars: 50 μm.

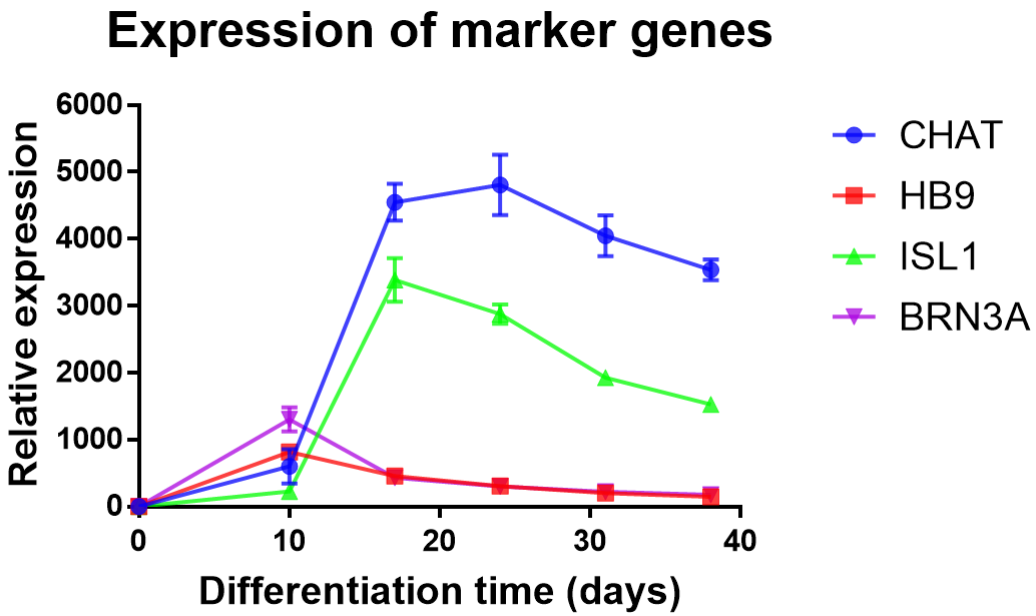

Figure 4. Gene expression analysis up to 38 days after motor neuron induction.

Expression levels of motor neuron markers ChAT, HB9, ISL1, and BRN3A are shown as relative expression. Gene expression values were normalized using the GAPDH gene expression values. N = 3, mean ± SD, for each gene.

A

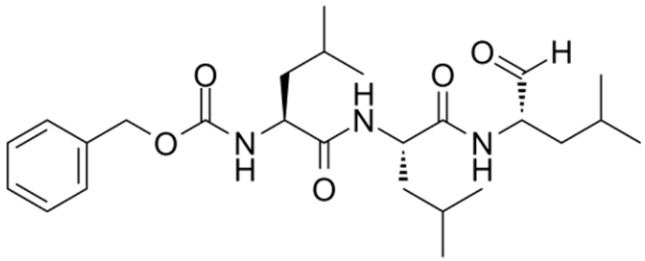
O
H
O
O
H
N
O
N
H
O
N
H

B

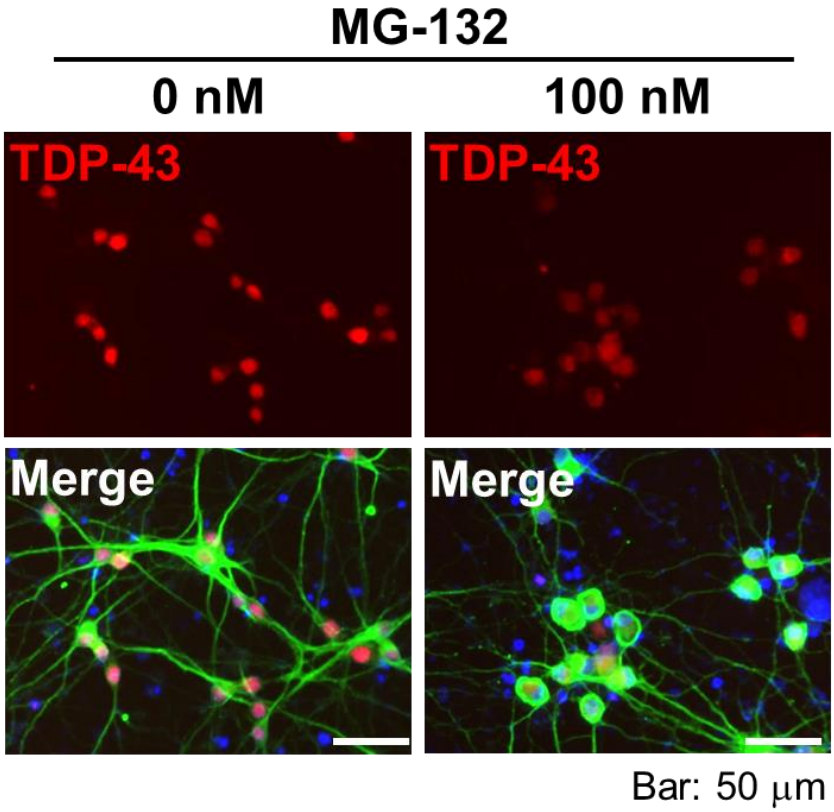
MG-132
0 nM
100 nM
TDP-43
TDP-43
Merge
Merge
Bar: 50 μm

Figure 5. Localization changes of TDP-43 by MG-132 treatment.

(A) Chemical structure of MG-132. (B) Images of TDP-43 expression in the motor neurons with or without 100 nM MG-132 treatment for 3 days. TDP-43, mKate2-TDP-43 expression; merge, merge of MAP2, mKate2-TDP-43, and Hoechst 33342. Scale bars: 50 μm.

A

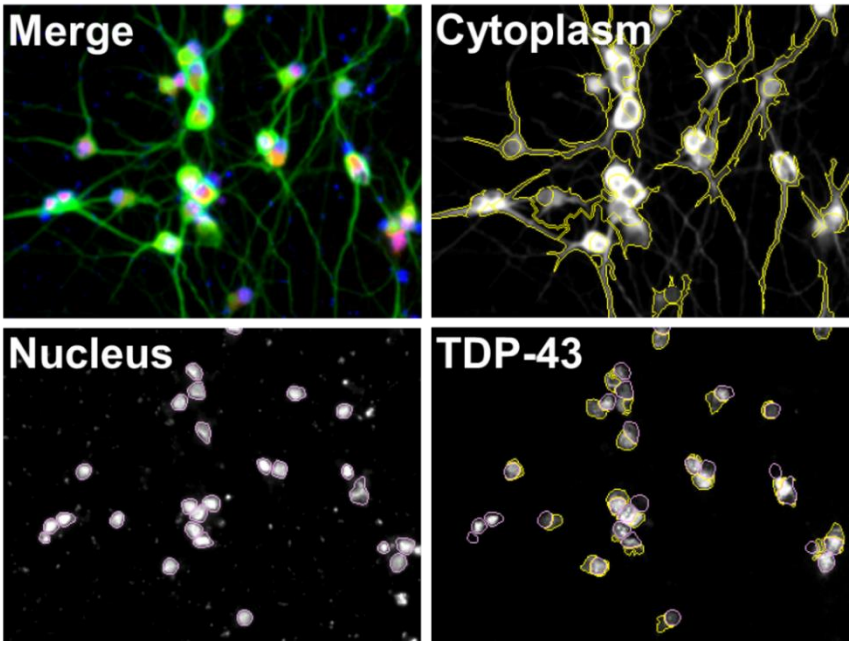
Merge
Cytoplasm
Nucleus
TDP-43

B

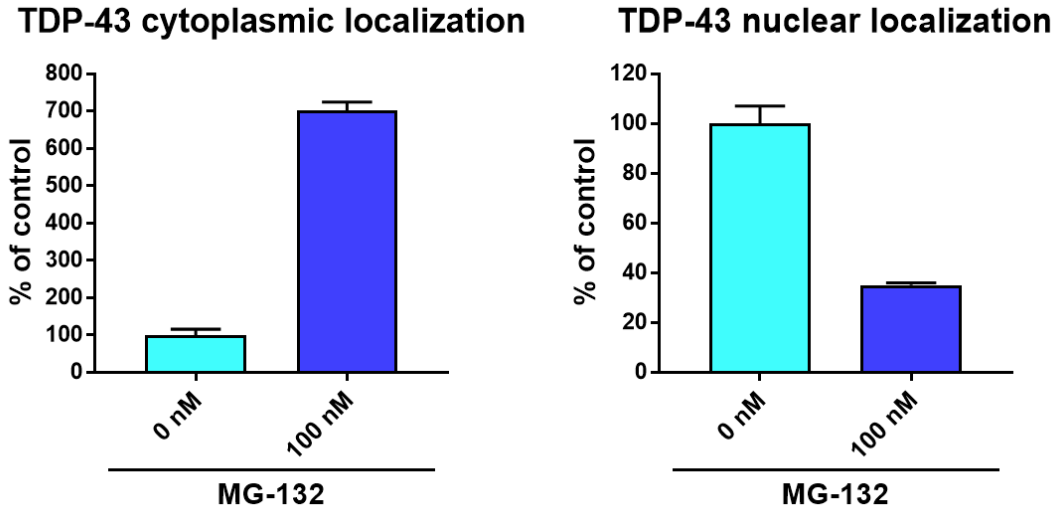
TDP-43 cytoplasmic localization
% of control
800
700
600
500
400
300
200
100
0
0 nM
100 nM
MG-132
TDP-43 nuclear localization
% of control
120
100
80
60
40
20
0
0 nM
100 nM
MG-132

Figure 6. Analysis of the cytoplasmic and nuclear localization of TDP-43.

(A) Cell images of recognition of cytoplasmic and nuclear regions of TDP-43. Merge, overlay of anti-MAP2, mKate2-TDP-43, and Hoechst 33342 images; cytoplasm, cytoplasmic regions were identified based on the staining of anti-MAP2, and yellow lines indicate the extent of image recognition by anti-MAP2 staining; nucleus, nuclear regions were identified based on the staining of Hoechst 33342; TDP-43, TDP-43 expression was divided into cytoplasmic and nuclear regions. (B) Measurement of TDP-43 localization changes in the cytoplasm and nucleus after treatment with or without 100 nM MG-132 for 3 days. N = 6, mean ± SD.

A

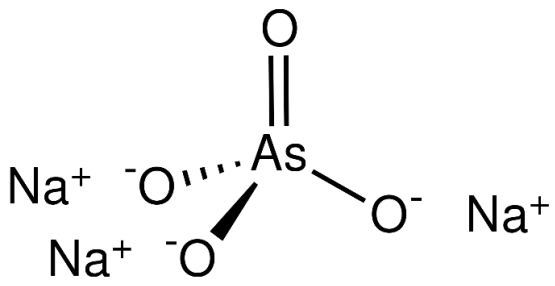
O
As
Na+ -O
O- Na+
Na+ -O

B

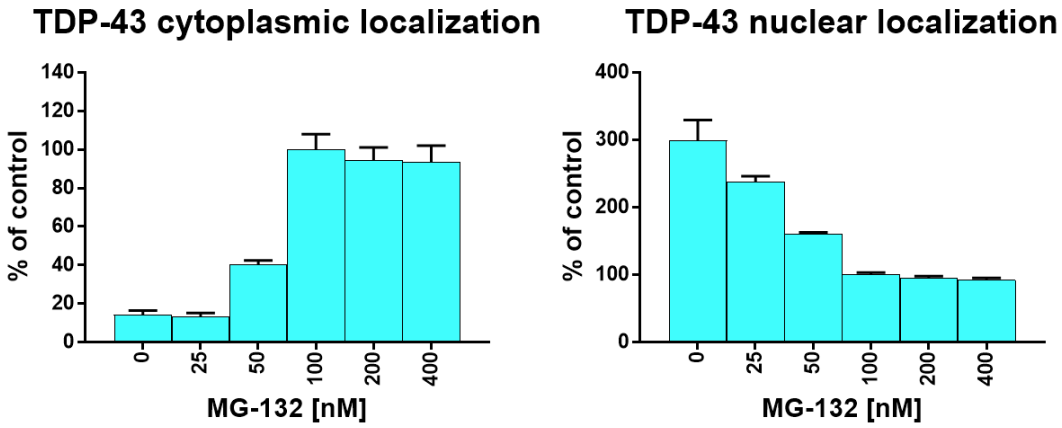
TDP-43 cytoplasmic localization
% of control
140
120
100
80
60
40
20
0
0
25
50
100
200
400
MG-132 [nM]
TDP-43 nuclear localization
% of control
400
300
200
100
0
0
25
50
100
200
400
MG-132 [nM]

C

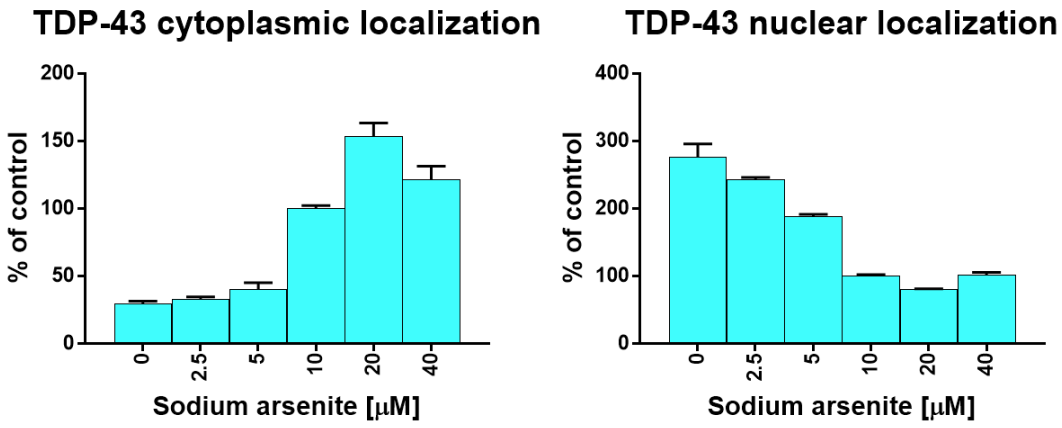
TDP-43 cytoplasmic localization
% of control
200
150
100
50
0
0
2.5
5
10
20
40
Sodium arsenite [μM]
TDP-43 nuclear localization
% of control
400
300
200
100
0
0
2.5
5
10
20
40
Sodium arsenite [μM]

Figure 7. Concentration dependency of MG-132 and sodium arsenite on TDP-43 localization changes.

(A) Chemical structure of sodium arsenite. (B) Measurement of TDP-43 localization changes in the cytoplasm and nucleus after treatment with MG-132 (0-400 nM) for 3 days. N = 3, mean ± SD. (C) Measurement of TDP-43 localization changes in the cytoplasm and nucleus after treatment with sodium arsenite (0-40 μM) for 1 days. N = 3, mean ± SD.

A

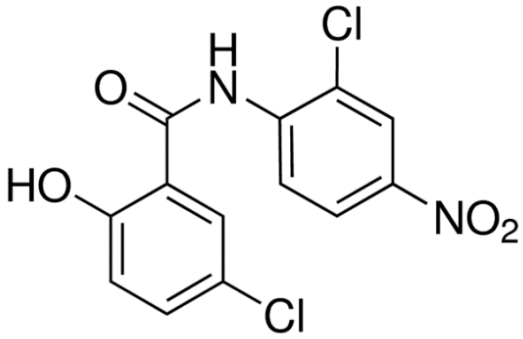

B

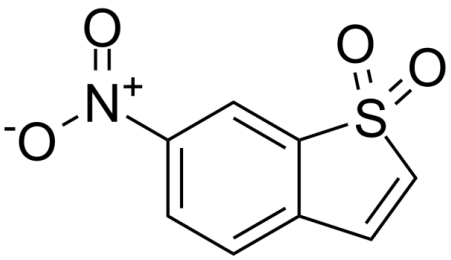

Figure 8. Chemical structure of niclosamide and stattic.

(A) Chemical structure of niclosamide. (B) Chemical structure of stattic.

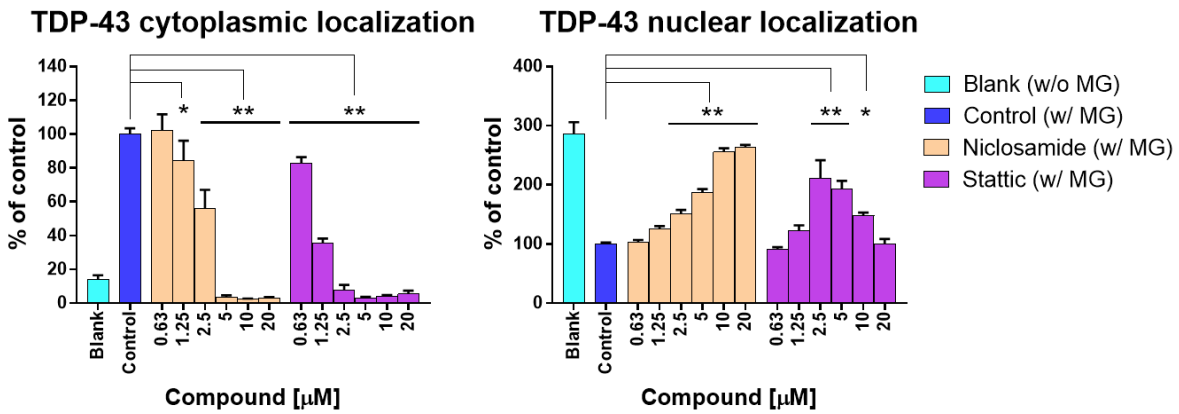

Figure 9. Niclosamide and stattic inhibit TDP-43 cytoplasmic and nuclear localization changes after treatment with 100 nM MG-132.

Measurement of TDP-43 localization changes in the cytoplasm and nucleus after treatment with 100 nM MG-132, and niclosamide or stattic for 3 days. Blank, without MG-132; control, 100 nM MG-132; niclosamide, 100 nM MG-132 with 0.63-20 μM niclosamide; stattic, 100 nM MG-132 with 0.63-20 μM stattic. N = 3, mean ± SD. *P < 0.01, **P < 0.001 vs. control, Tukey's multiple comparison test.

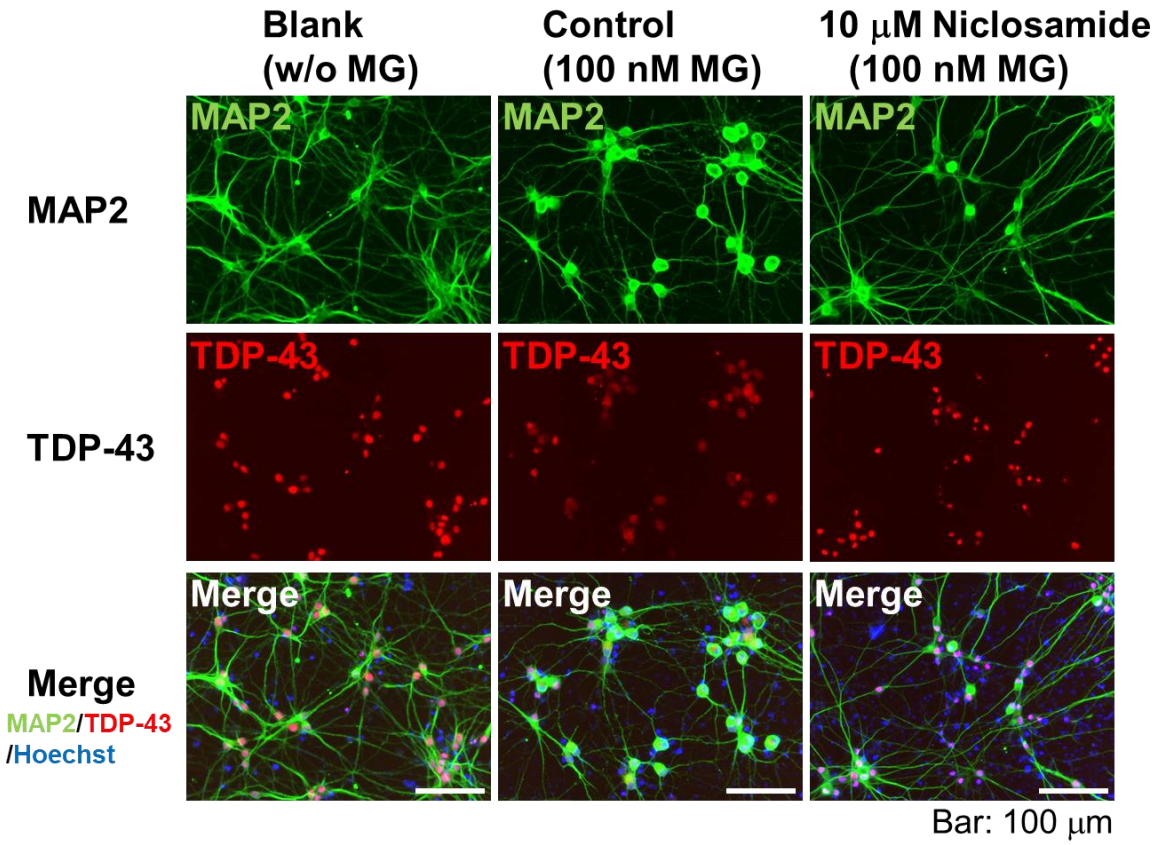

Figure 10. Immunocytochemical analysis after treatment with 100 nM MG-132 and 10 μM niclosamide for 3 days.

Blank, without MG-132; control, 100 nM MG-132; 10 μM niclosamide, 100 nM MG-132 with 10 μM niclosamide. Fluorescence images of anti-MAP2 (upper), mKate2-TDP-43 (middle), merge of MAP2, mKate2-TDP-43, and Hoechst 33342 (lower). Scale bars: 100 μm.

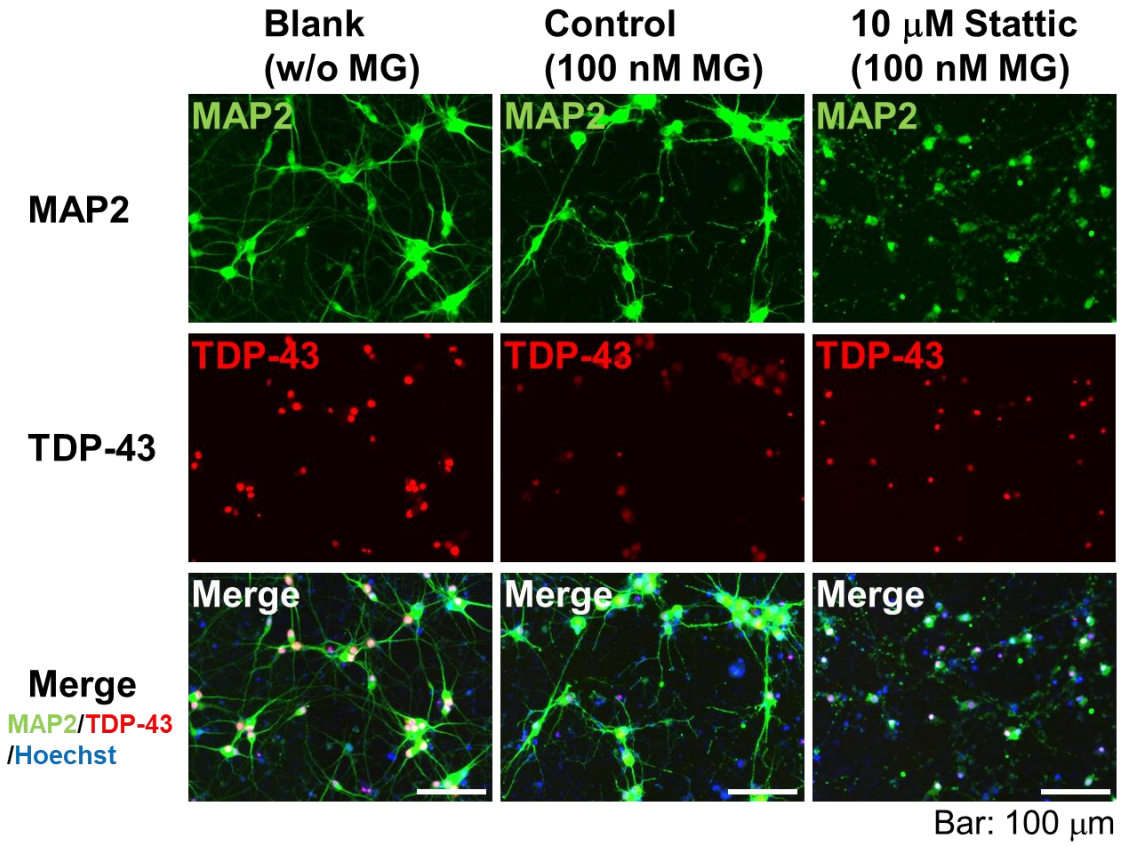

Figure 11. Immunocytochemical analysis after treatment with 100 nM MG-132 and 10 μM stattic for 3 days.

Blank, without MG-132; control, 100 nM MG-132; 10 μM stattic, 100 nM MG-132 with 10 μM stattic. Fluorescence images of anti-MAP2 (upper), mKate2-TDP-43 (middle), merge of MAP2, mKate2-TDP-43, and Hoechst 33342 (lower). Scale bars: 100 μm.

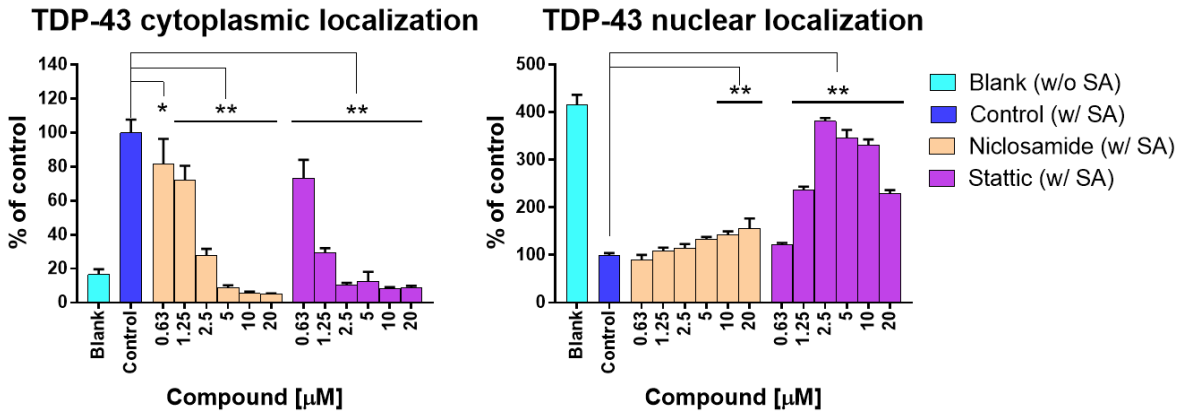

Figure 12. Niclosamide and stattic inhibit TDP-43 cytoplasmic and nuclear localization changes after treatment with 10 μM sodium arsenite.

Measurement of TDP-43 localization changes in the cytoplasm and nucleus after treatment with 10 μM sodium arsenite, and niclosamide or stattic for 1 day. Blank, without sodium arsenite; control, 10 μM sodium arsenite; niclosamide, 10 μM sodium arsenite with 0.63-20 μM niclosamide; stattic, 10 μM sodium arsenite with 0.63-20 μM stattic. N=3, mean ± SD. *P < 0.01, **P < 0.001 vs. control, Tukey's multiple comparison test.

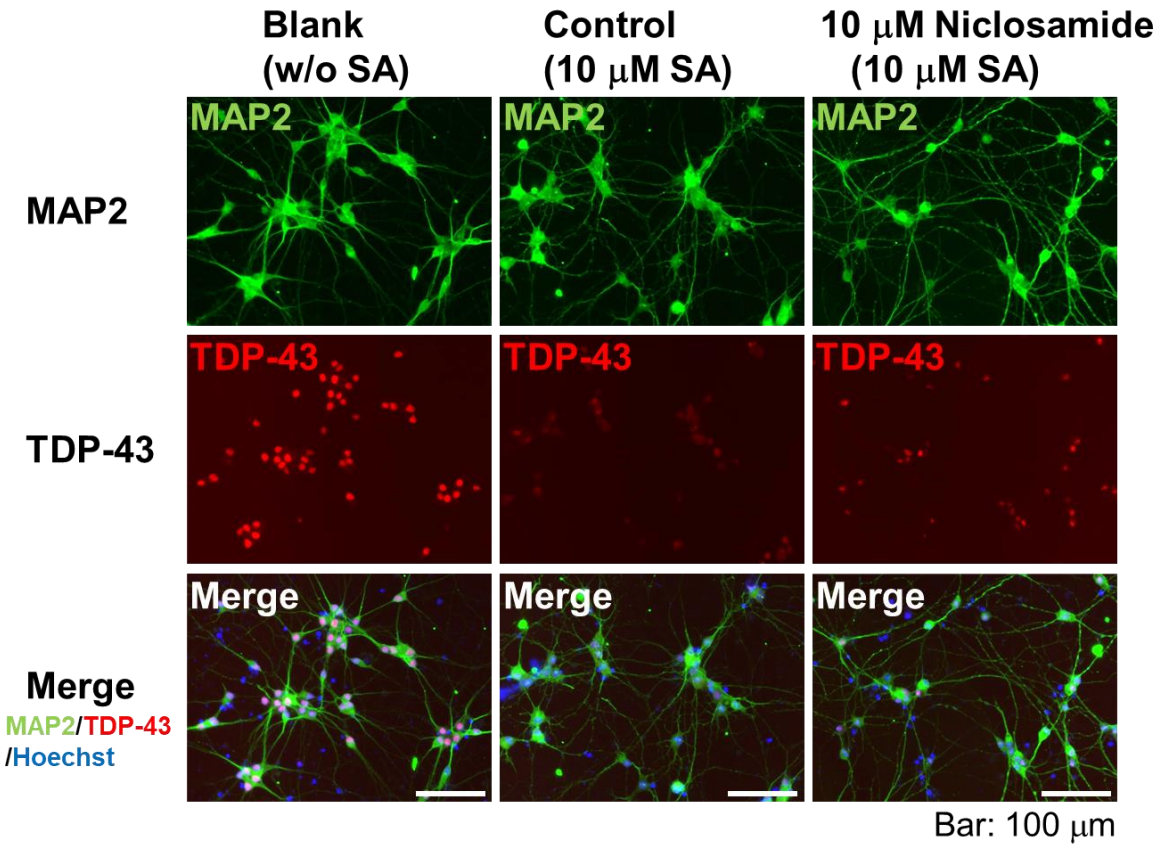

Figure 13. Immunocytochemical analysis after treatment with 10 μM sodium arsenite and 10 μM niclosamide for 1 day.

Blank, without sodium arsenite; control, 10 μM sodium arsenite; 10 μM niclosamide, 10 μM sodium arsenite with 10 μM niclosamide. Fluorescence images of anti-MAP2 (upper), mKate2-TDP-43 (middle), merge of MAP2, mKate2-TDP-43, and Hoechst 33342 (lower). Scale bars: 100 μm.

A

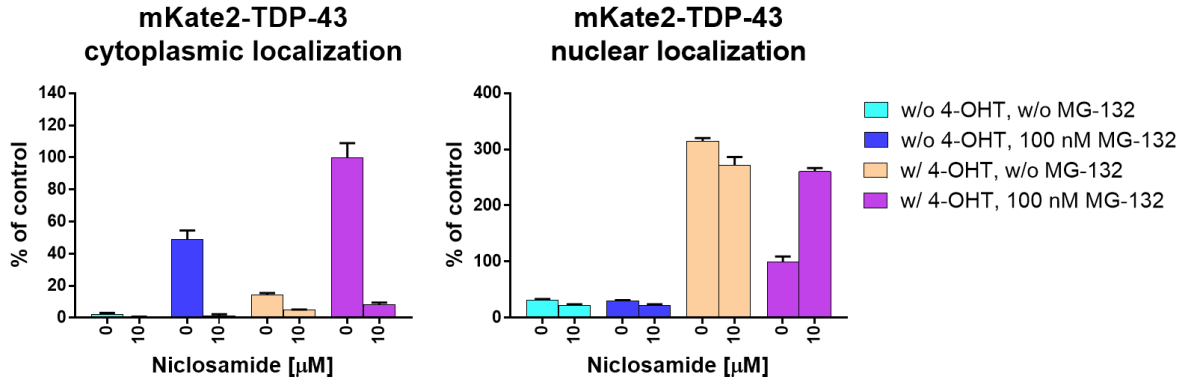
mKate2-TDP-43
cytoplasmic localization
mKate2-TDP-43
nuclear localization
% of control
Niclosamide [μM]
w/o 4-OHT, w/o MG-132
w/o 4-OHT, 100 nM MG-132
w/ 4-OHT, w/o MG-132
w/ 4-OHT, 100 nM MG-132

B

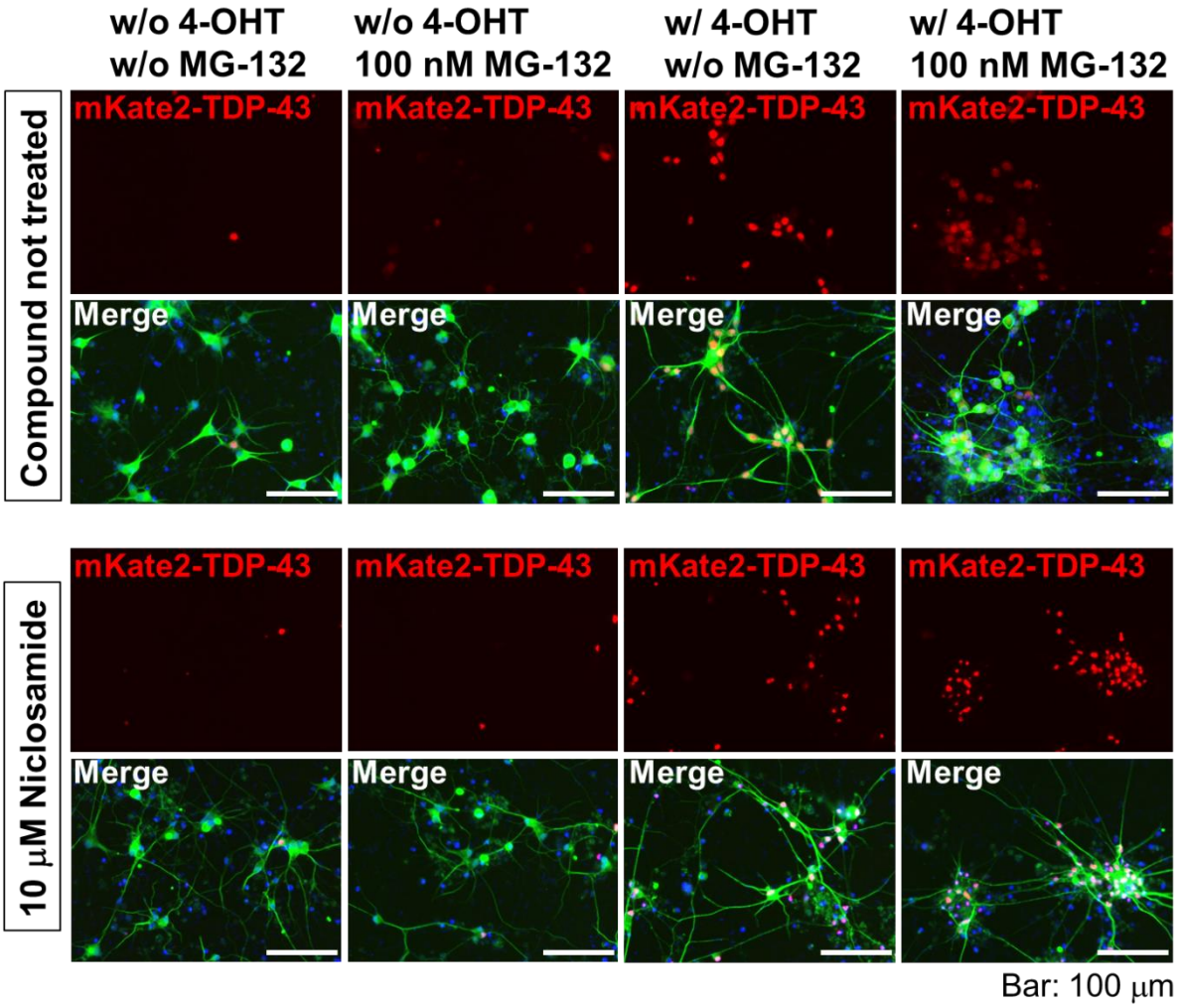
w/o 4-OHT
w/o MG-132
w/o 4-OHT
100 nM MG-132
w/ 4-OHT
w/o MG-132
w/ 4-OHT
100 nM MG-132
Compound not treated
10 μM Niclosamide
mKate2-TDP-43
Merge
Bar: 100 μm

Figure 14. TDP-43 localization changes under the different induction conditions of 4-OHT and MG-132.

(A) Measurement of TDP-43 localization changes in the cytoplasm and nucleus after treatment with or without 100 nM 4-OHT for 4 days, and then with or without 100 nM MG-132, and 10 μM niclosamide for 3 days. w/o 4-OHT, without 4-OHT; w/ 4-OHT, 100 nM 4-OHT; w/o MG-132, without MG-132. N = 3, mean ± SD. (B) Immunocytochemical analysis after treatment with or without 100 nM 4-OHT for 4 days, and then with or without 100 nM MG-132, and 10 μM niclosamide for 3 days. Fluorescence images of mKate2-TDP-43 (upper), merge of MAP2, mKate2-TDP-43, and Hoechst 33342 (lower). Scale bars: 100 μm.

A

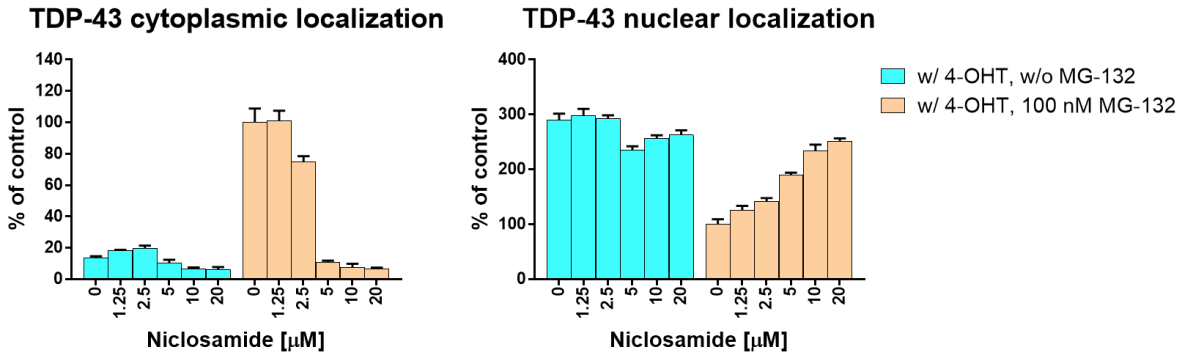
TDP-43 cytoplasmic localization
TDP-43 nuclear localization
% of control
Niclosamide [μM]
w/ 4-OHT, w/o MG-132
w/ 4-OHT, 100 nM MG-132

B

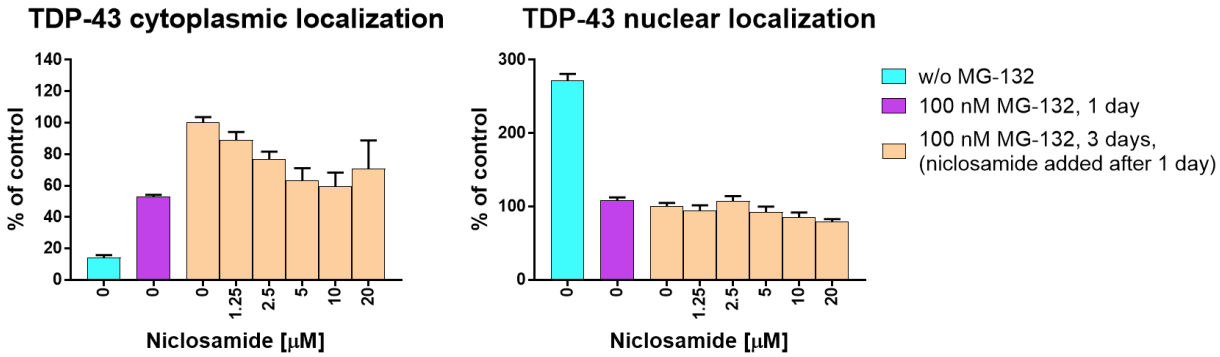
TDP-43 cytoplasmic localization
TDP-43 nuclear localization
% of control
Niclosamide [μM]
w/o MG-132
100 nM MG-132, 1 day
100 nM MG-132, 3 days,
(niclosamide added after 1 day)

Figure 15. TDP-43 localization changes by niclosamide in different addition methods.

(A, B) Measurement of TDP-43 localization changes in the cytoplasm and nucleus. (A) Effect of niclosamide with or without MG-132. With 100 nM 4-OHT for 4 days, and then with or without 100 nM MG-132, and niclosamide (0-20 μM) for 3 days. w/ 4-OHT, 100 nM 4-OHT; w/o MG-132, without MG-132. N = 3, mean ± SD. (B) Addition of MG-132 prior to niclosamide treatment. Cells were treated with 100 nM 4-OHT for 4 days, with 100 nM MG-132 for 1 day, followed by addition of MG-132 and niclosamide (0-20 μM) for 2 days. w/o MG-132, without MG-132. N = 3, mean ± SD.

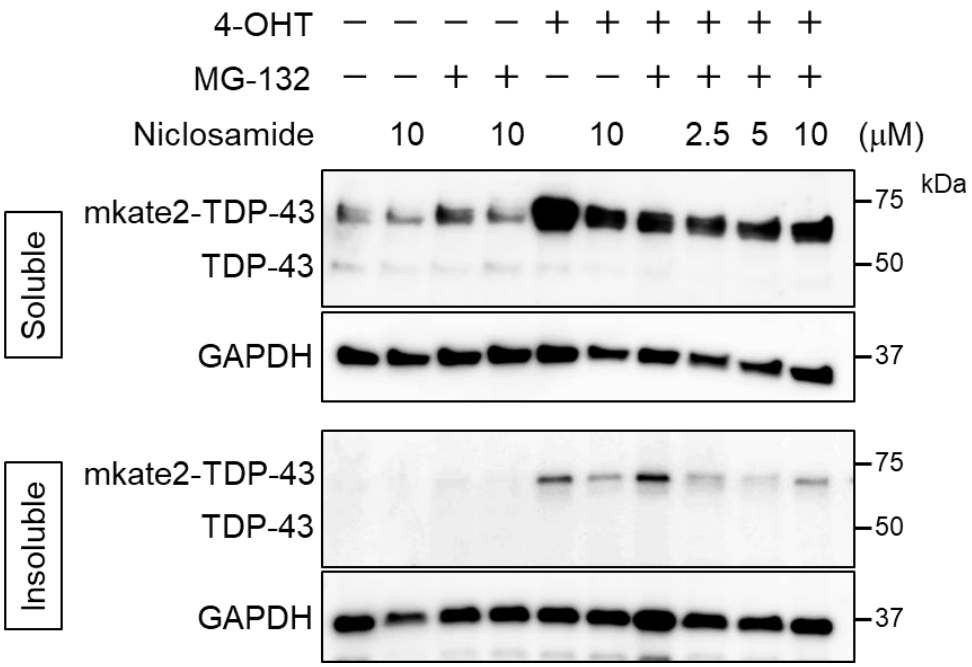

Figure 16. TDP-43 expression separated into soluble and insoluble fractions.

Western blot analysis fractionated into soluble and insoluble TDP-43 after treatment with or without 100 nM 4-OHT for 4 days, and then with or without 100 nM MG-132, and niclosamide (2.5-10 μM) for 3 days. Western blots were probed with anti-TDP-43 and anti-GAPDH.

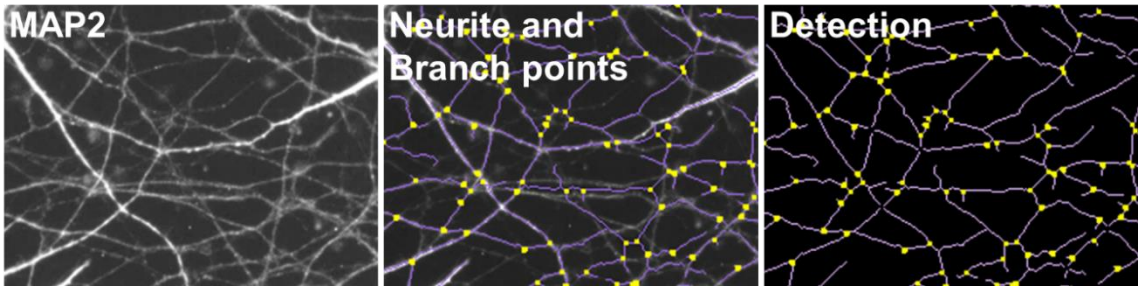

Figure 17. Cell images of neurite staining with anti-MAP2.

MAP2, fluorescence images of anti-MAP2; neurite and branch points, recognition of the neurite (purple) and branch points (yellow) from anti-MAP2 stained images; detection, detection of the neurite (purple) and branch points (yellow).

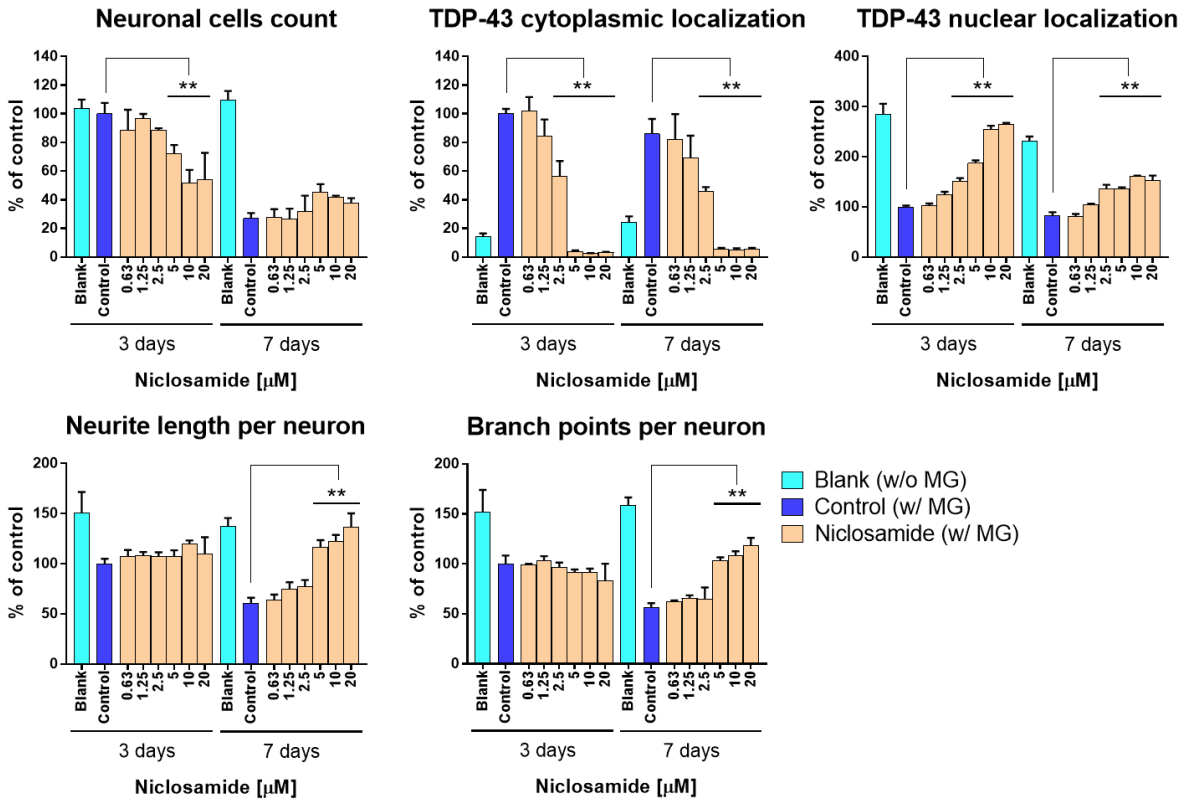

Figure 18. Niclosamide attenuates morphological changes under stress.

Determination of neuronal cell count, TDP-43 localization changes in the cytoplasm and nucleus, neurite length per neuron, and the number of branch points per neuron after treatment with 100 nM MG-132 and niclosamide for 3 days or 7 days. Blank, without MG-132; control, 100 nM MG-132; niclosamide, 100 nM MG-132 with 0.63-20 μM niclosamide. N = 3, mean ± SD. **P < 0.001 vs. control, Tukey's multiple comparison test.

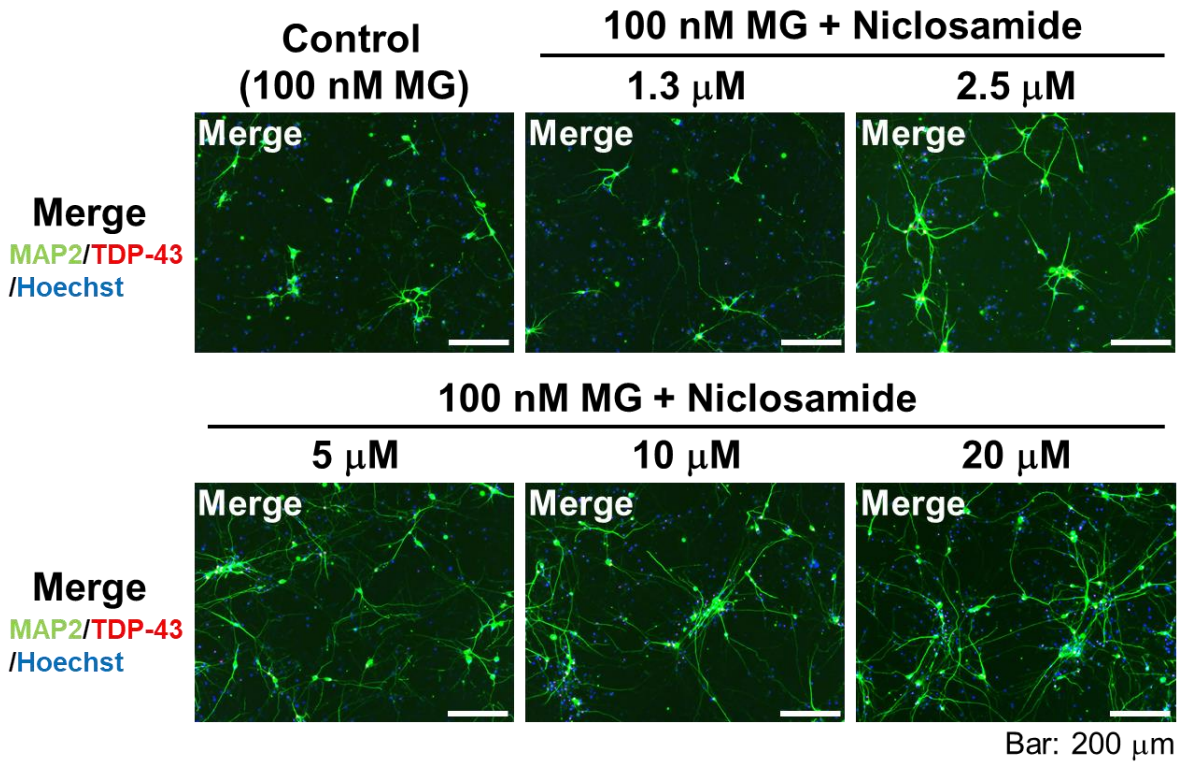

Figure 19. Immunocytochemical analysis after treatment with 100 nM MG-132 and niclosamide for 7 days.

Control, 100 nM MG-132; 1.3-20 μM niclosamide, 100 nM MG-132 with 1.3-20 μM niclosamide. Merged fluorescence images of anti-MAP2, mKate2-TDP-43, and Hoechst 33342. Scale bars: 200 μm.

A

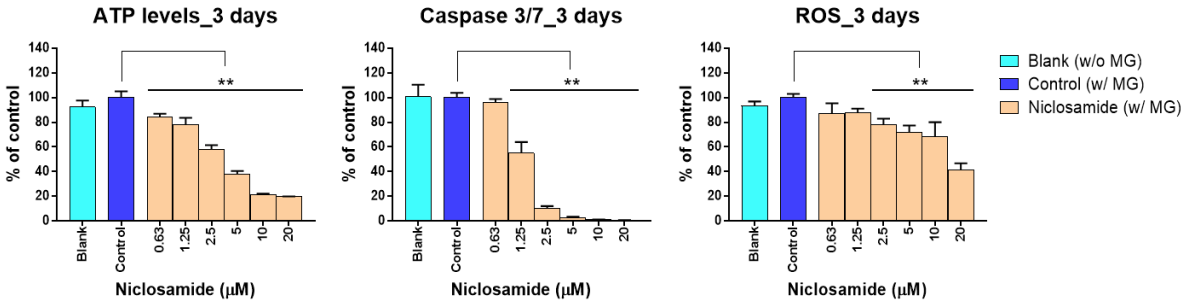
ATP levels_3 days
Caspase 3/7_3 days
ROS_3 days
% of control
Blank
Control
0.63
1.25
2.5
5
10
20
Niclosamide (μM)
**
Blank (w/o MG)
Control (w/ MG)
Niclosamide (w/ MG)

B

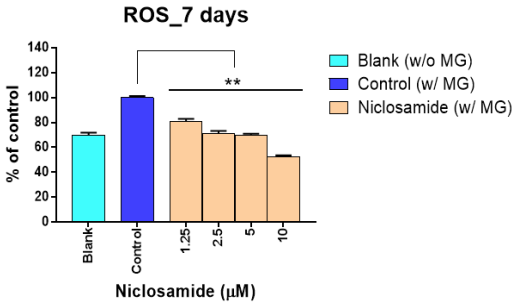
ROS_7 days
% of control
Blank
Control
1.25
2.5
5
10
Niclosamide (μM)
**
Blank (w/o MG)
Control (w/ MG)
Niclosamide (w/ MG)

Figure 20. Niclosamide decreases intracellular ATP and suppressed ROS production.

(A) Intracellular ATP levels, caspase 3/7 activities, and ROS (H_2O_2) production in cells were measured after treatment with 100 nM MG-132 and niclosamide for 3 days. (B) Intracellular ROS (H_2O_2) production in cells were measured after treatment with 100 nM MG-132 and niclosamide for 7 days. (A, B) Blank, without MG-132; control, 100 nM MG-132; niclosamide, 100 nM MG-132 with 0.63-20 μM niclosamide. N = 3, mean ± SD. **P < 0.001 vs control, Tukey's multiple comparison test.

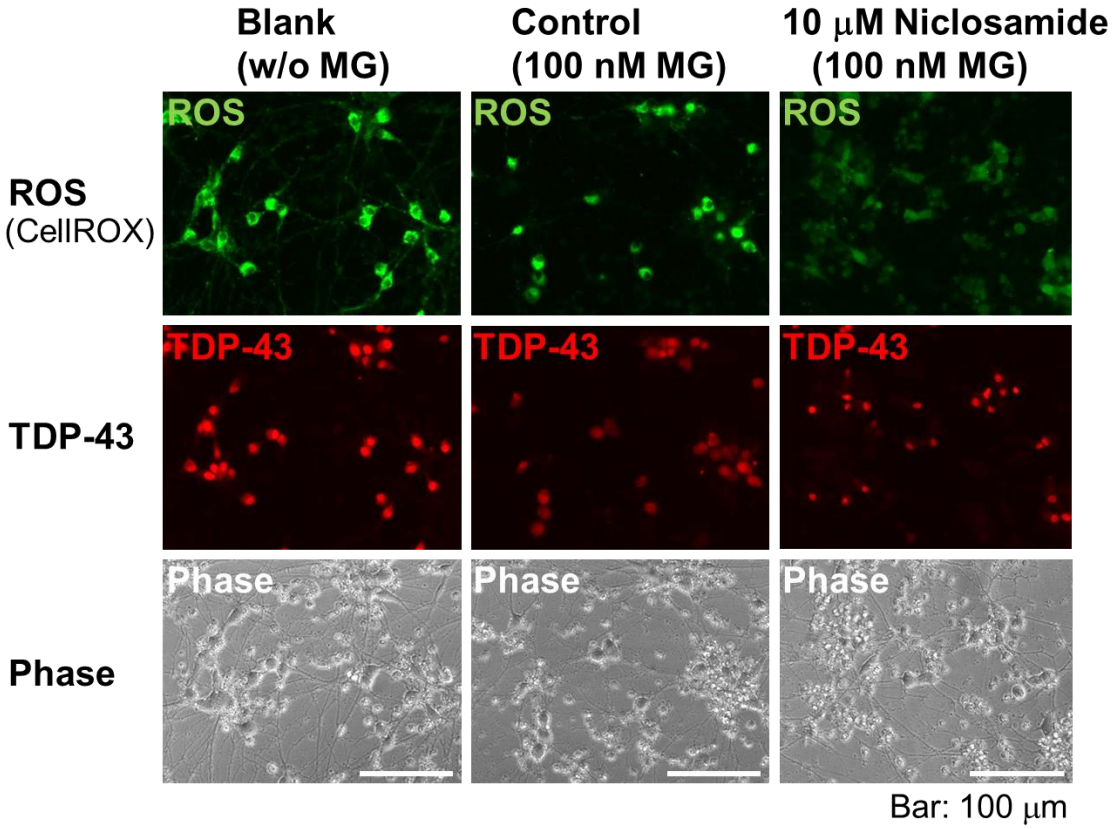

Figure 21. Cell images of intracellular ROS by direct fluorescence detection using CellROX reagent after treatment with 100 nM MG-132 and niclosamide for 1 day.

Blank, without MG-132; control, 100 nM MG-132; 10 μM niclosamide, 100 nM MG-132 with 10 μM niclosamide. The images of CellROX detection (upper), fluorescence of mKate2-TDP-43 (middle), phase contrast (lower). Scale bars: 100 μm.

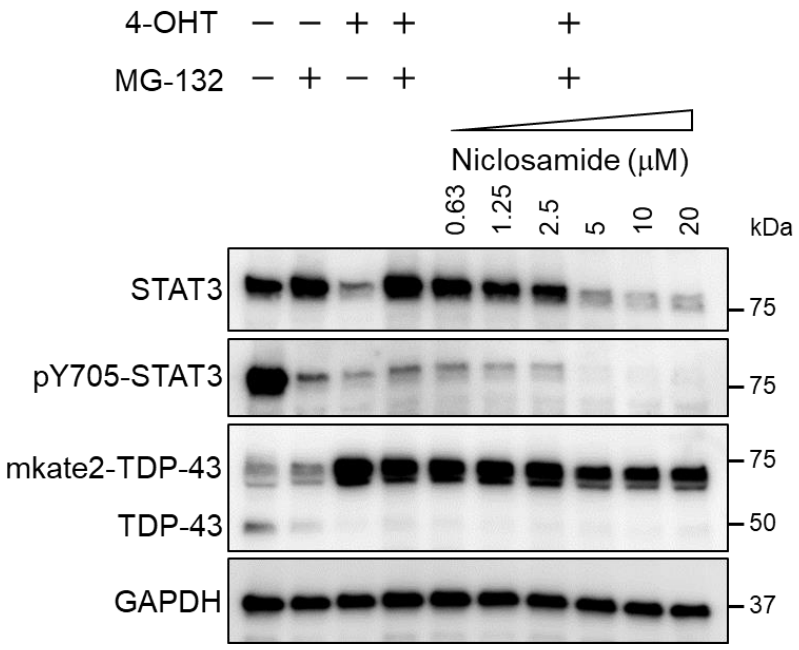

Figure 22. Niclosamide inhibits STAT3 phosphorylation.

Western blot analysis after treatment with or without 100 nM 4-OHT for 4 days, and then with or without 100 nM MG-132, and niclosamide (0.63-20 μM) for 3 days. Western blots were probed with anti-STAT3, anti-phospho-STAT3 (Tyr705), anti-TDP-43, and anti-GAPDH.

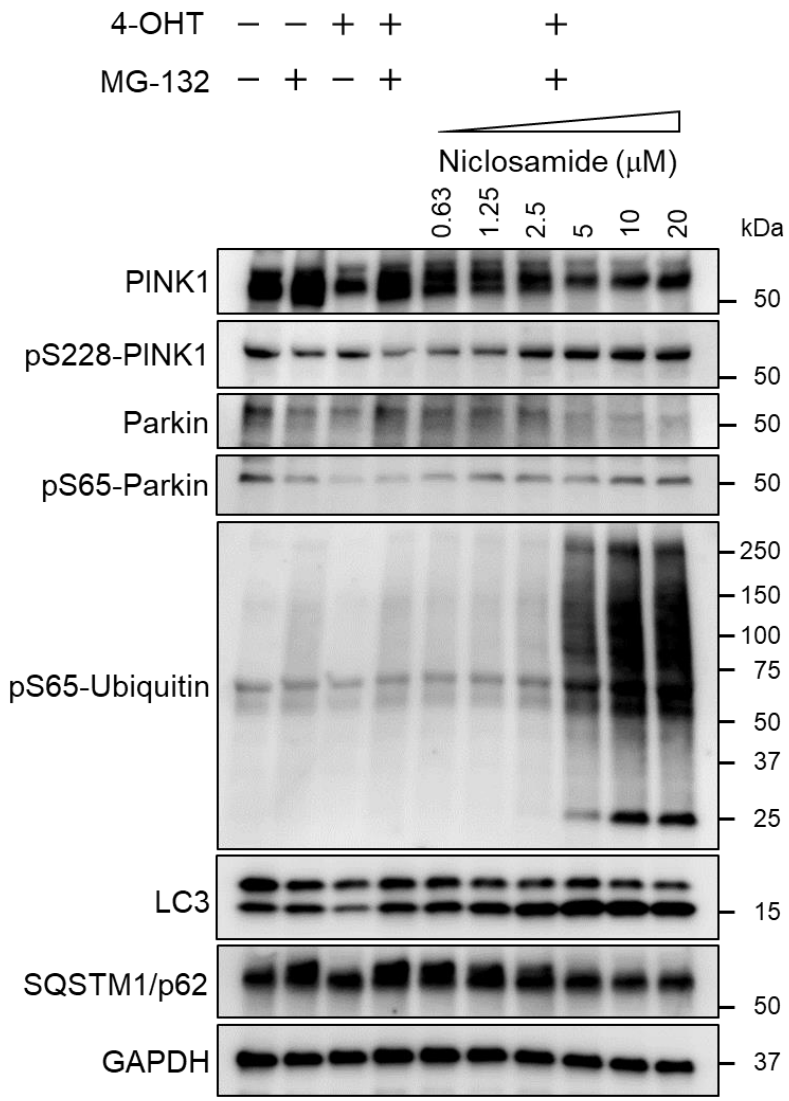

Figure 23. Niclosamide activates PINK1-parkin-ubiquitin pathway to induce mitophagy and autophagy.

Western blot analysis after treatment with or without 100 nM 4-OHT for 4 days, and then with or without 100 nM MG-132, and niclosamide (0.63-20 μM) for 3 days. Western blots were probed with anti-PINK1, anti-phospho-PINK1 (Ser228), anti-parkin, anti-phospho-parkin (Ser65), anti-phospho-ubiquitin (Ser65), anti-LC3, anti-SQSTM1/p62, and anti-GAPDH.

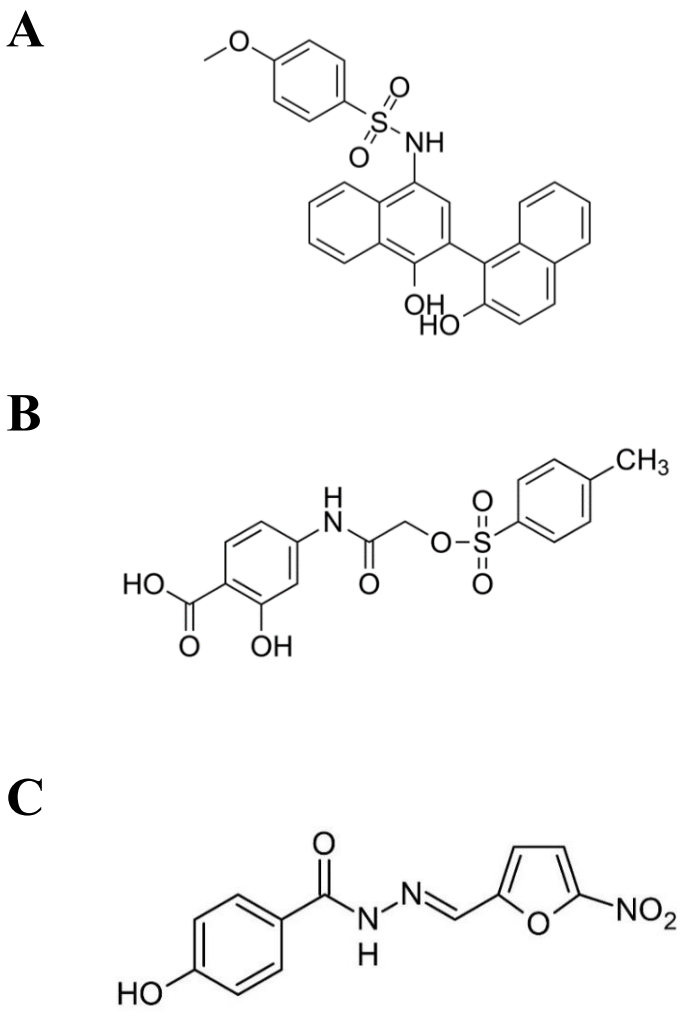

Figure 24. Chemical structure of C188-9, S3I-201, and nifuroxazide.

(A) Chemical structure of C188-9. (B) Chemical structure of S3I-201. (C) Chemical structure of nifuroxazide.

A

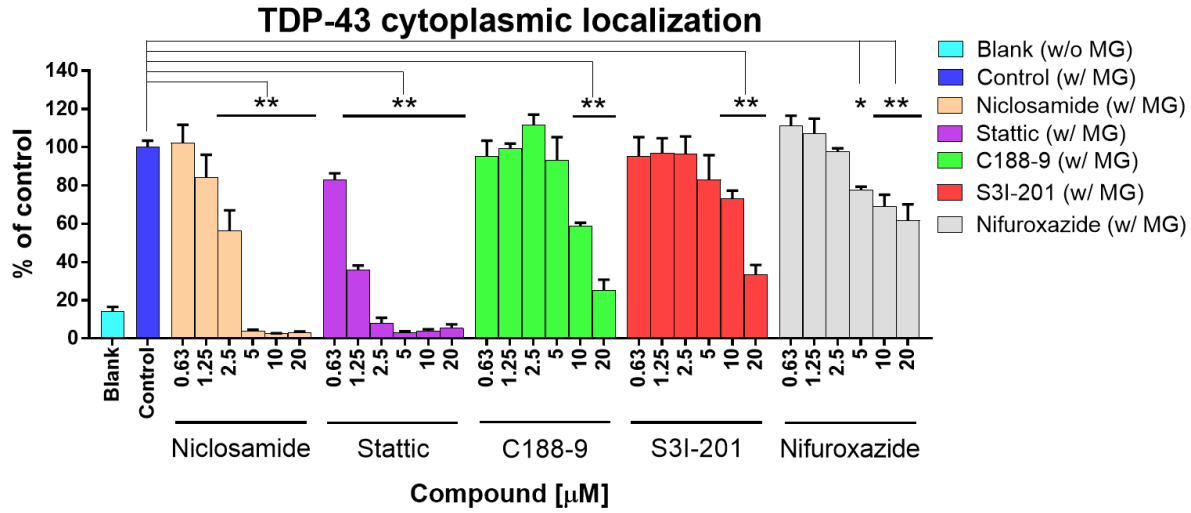
TDP-43 cytoplasmic localization
% of control
Blank (w/o MG)
Control (w/ MG)
Niclosamide (w/ MG)
Stattic (w/ MG)
C188-9 (w/ MG)
S3I-201 (w/ MG)
Nifuroxazide (w/ MG)
Niclosamide
Stattic
C188-9
S3I-201
Nifuroxazide
Compound [μM]

B

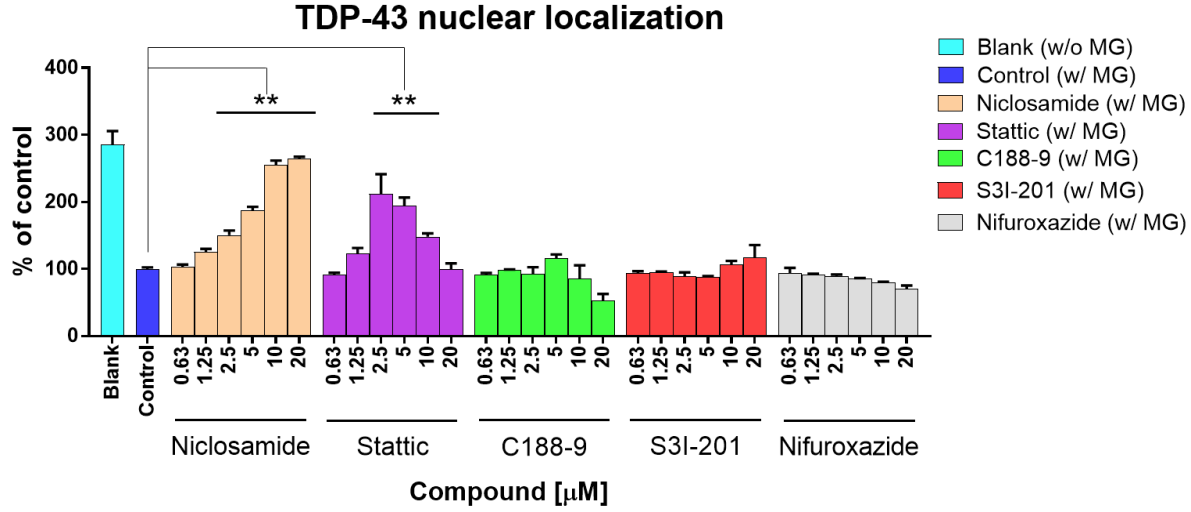
TDP-43 nuclear localization
% of control
Blank (w/o MG)
Control (w/ MG)
Niclosamide (w/ MG)
Stattic (w/ MG)
C188-9 (w/ MG)
S3I-201 (w/ MG)
Nifuroxazide (w/ MG)
Niclosamide
Stattic
C188-9
S3I-201
Nifuroxazide
Compound [μM]

Figure 25. Measurement of TDP-43 localization changes in the cytoplasm and nucleus after treatment with 100 nM MG-132 and STAT3 inhibitors (niclosamide, stattic, C188-9, S3I-201, or nifuroxazide) for 3 days.

(A) Measurement of TDP-43 localization changes in the cytoplasm. (B) Measurement of TDP-43 localization changes in the nucleus. (A, B) Blank, without MG-132; control, 100 nM MG-132; STAT3 inhibitors, 100 nM MG-132 with 0.63-20 μM compounds. N = 3, mean ± SD. *P < 0.01, **P < 0.001 vs control, Tukey's multiple comparison test.

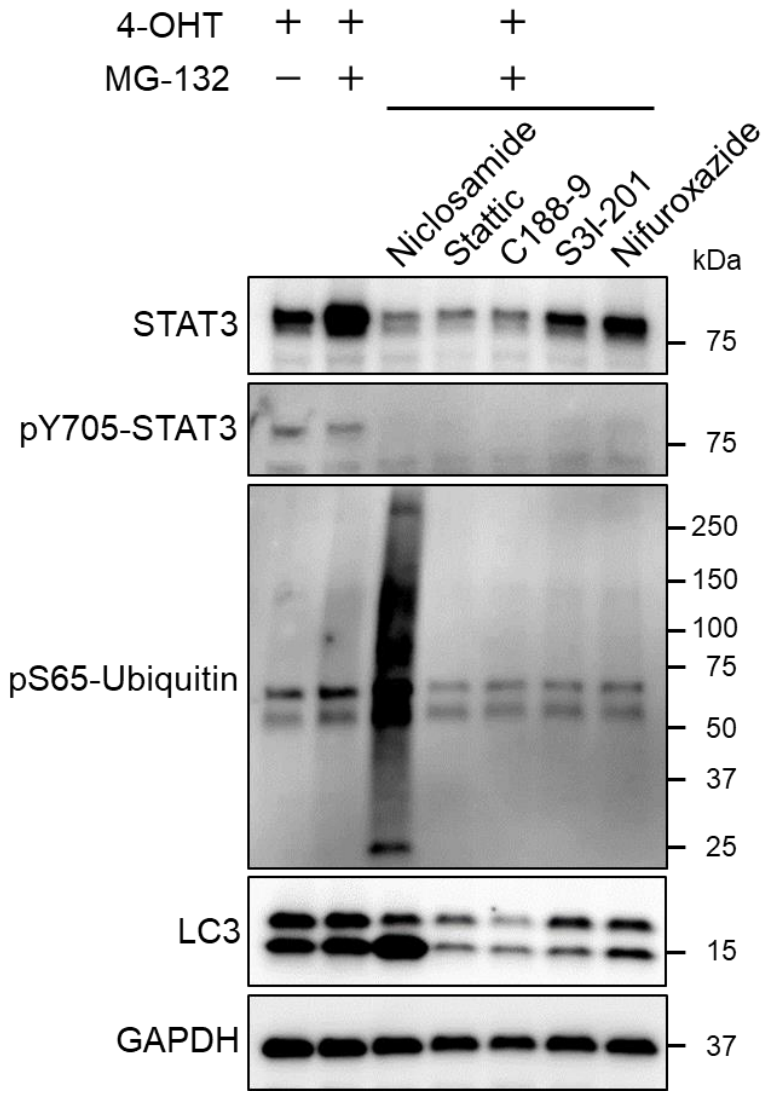

Figure 26. Only niclosamide among STAT3 inhibitors activates mitophagy and autophagy.

Western blot analysis after treatment with 100 nM 4-OHT for 4 days, and then with or without 100 nM MG-132, and 10 μM STAT3 inhibitors (niclosamide, stattic, C188-9, S3I-201, nifuroxazide) for 3 days. Western blots were probed with anti-STAT3, anti-phospho-STAT3 (Tyr705), anti-phospho-ubiquitin (Ser65), anti-LC3, and anti-GAPDH.